

The editor has absolutely right. Again the equation (14) is not correct. According with the editor the equation (14) has been corrected and assumes the following expression:

$$Q_j = \sum Q \frac{1}{R_j} \left(\sum_{i=1}^n \frac{1}{R_i} \right)^{-1}$$

Where the following term:

$$\left(\sum_{i=1}^n \frac{1}{R_i} \right)^{-1}$$

Represents the total resistance term equal to the inverse of the reciprocal of the sum of the each resistance term.

However in the paper the equation (14) is not directly used. In fact the equation (29) is derived by applying directly the first and second Kirchhoff laws.

For the simplest case of two resistances the equation (14) and equation (29) are equivalent. In fact:

$$\begin{aligned} Q_j &= \sum Q \frac{1}{R_j} \left(\sum_{i=1}^n \frac{1}{R_i} \right)^{-1} \Rightarrow Q_1 = Q_0 \frac{1}{R_6} \left(\frac{1}{R_6} + \frac{1}{R_3 + R_4 + R_5} \right)^{-1} \Rightarrow \\ &\Rightarrow Q_1 = Q_0 \frac{1}{R_6} \frac{R_6(R_3 + R_4 + R_5)}{R_3 + R_4 + R_5 + R_6} \Rightarrow Q_1 = Q_0 \frac{R_3 + R_4 + R_5}{R_3 + R_4 + R_5 + R_6} \end{aligned}$$

~~On~~ On the reliability of analytical models to predict solute transport in a fracture network

Claudia Cherubini*, Concetta I. Giasi**, Nicola Pastore**

*HydrISE, Institut Polytechnique LaSalle Beauvais, 19 rue Pierre Waguët, 60026 Beauvais Cedex, France

** Polytechnical University of Bari, Bari, Italy

Abstract

In hydrogeology, the application of reliable tracer transport model approaches is a key issue to derive the hydrodynamic properties of aquifers.

Laboratory and field – scale tracer dispersion breakthrough curves (BTC) in fractured media are notorious for exhibiting early time arrivals and late – time tailing that are not captured by the classical advection – dispersion equation (ADE). These “non – Fickian” features are proved to be better explained by a mobile – immobile (MIM) approach. In this conceptualization the fractured rock system is schematized as a continuous medium in which the liquid phase is separated into flowing and stagnant regions.

The present study compares the performances and reliabilities of ~~the~~ classical Mobile – Immobile Model (MIM) and the Explicit Network Model (ENM) that takes expressly into account the network geometry for describing tracer transport ~~behavior~~ behaviour in a fractured sample at bench scale. Though ENM shows better fitting results than MIM, the latter remains still valid as it proves to describe the observed curves quite well.

The results show that the presence of nonlinear flow plays an important role ~~in~~ the behaviour of solute transport. First~~ly~~ the distribution of solute according to different pathways is not constant but ~~it~~ is related to the flow rate. Second~~ly~~ nonlinear flow influences advection, in that it leads to a delay in solute transport respect to the linear flow assumption. Whereas nonlinear flow does not show to be related with dispersion. The experimental results show that in the study case the geometrical dispersion dominates the Taylor dispersion. However the interpretation with the ENM model shows a weak transitional regime from geometrical dispersion to Taylor dispersion for high flow rates. ~~The experimental results show that in the study case the geometrical dispersion dominates the Taylor~~

~~dispersion~~. Incorporating the description of the flowpaths in the analytical modeling has proved to better fit the curves and to give a more robust interpretation of the solute transport.

Introduction

In fractured rock formations, the rock mass hydraulic ~~behavior~~behaviour is controlled by fractures. In such aquifers, open and well – connected fractures constitute high permeability pathways and are orders of magnitude more permeable than the rock matrix (Bear & Berkowitz, 1987; Berkowitz, 2002; Bodin et al., 2003; Cherubini, 2008; Cherubini & Pastore, 2011, Geiger et al., 2012, Neuman, 2005).

Formatted: English (U.K.)

In most studies examining hydrodynamic processes in fractured media, it is assumed that flow is described by Darcy's law, which expresses a linear relationship between pressure gradient and flow rate (Cherubini & Pastore, 2010). Darcy's law has been demonstrated to be valid at low flow regimes ($Re < 1$). For $Re > 1$ a nonlinear flow ~~behavior~~behaviour is likely to occur.

Formatted: English (U.K.)

But in real rock fractures, microscopic inertial phenomena can cause an extra macroscopic hydraulic loss (Kl v, 2000) which deviates flow from the linear relationship among pressure drop and flow rate.

To experimentally investigate ~~the~~ fluid flow regimes through deformable rock fractures, Zhang & Nemcik (2013) carried out flow tests through both mated and non – mated sandstone fractures in triaxial cell. For water flow through mated fractures, the experimental data confirmed the validity of linear Darcy's law at low velocity. For larger water flow through non – mated fractures, the relationship between pressure gradient and volumetric flow rate revealed that the Forchheimer equation offers a good description for this particular flow process. The obtained experimental data show that Izbash's law can also provide an excellent description for nonlinear flow. They concluded that further work was needed to study the dependency of the two coefficients on flow velocity. (forse va citato qualche altro paper sul flusso non darciano nelle fratture)

In fracture networks heterogeneity intervenes even in solute transport: due to the variable aperture and heterogeneities of the fracture surfaces the fluid flow will seek out preferential paths (Gylling et al., 1995) through which solutes are transported.

Generally the geometry of fracture network is not well known and the study of solute transport ~~behavior~~behaviour is based on multiple domain theory according to which the fractured medium is separated in two distinct domains: high velocity zones such as the network of connected fractures (mobile domain) where solute transport occurs predominantly by advection, and lower velocity

Formatted: English (U.K.)

60 zones such as secondary pathways, stagnation zones (almost – immobile domain), such as the rock
61 matrix.

62 Moreover, the presence of steep concentration gradients between fractures and matrix causes local
63 disequilibrium in solute concentration which gives rise to dominantly diffusive exchange between
64 fracture and matrix. This explains the non – Fickian nature of transport, which is characterized by
65 breakthrough curves with early first arrival and long tails.

66
67 Quantifying solute transport in fractured media has become a very challenging research topic in
68 hydrogeology over the last three decades (Nowamooz et al., 2013, Cherubini et al., 2009).

Formatted: English (U.K.)

69
70
71 ~~Therefore in the fracture network different pathways can be identified through which solute is~~
72 ~~generally distributed in function of the energy spent by solute particles to cross the path. In this~~
73 ~~context the presence of nonlinear flow plays an important role in the distribution of the solutes~~
74 ~~according to the different pathways. In fact the energy spent to cross the path is proportional to the~~
75 ~~resistance to flow associated to the single pathway, which in nonlinear flow regime is not constant~~
76 ~~but depends on the flow rate.~~

77 ~~This means that changing boundary conditions the resistance to flow varies and as a consequence~~
78 ~~the distribution of solute in the main and secondary pathways also changes giving rise to a different~~
79 ~~behaviour of solute transport. Moreover, the presence of steep concentration gradients between~~
80 ~~fractures and matrix causes local disequilibrium in solute concentration which gives rise to~~
81 ~~dominantly diffusive exchange between fracture and matrix. This explains the non – Fickian nature~~
82 ~~of transport, which is characterized by breakthrough curves with early first arrival and long tails.~~

83 ~~Quantifying solute transport in fractured media has become a very challenging research topic in~~
84 ~~hydrogeology over the last three decades (Nowamooz et al., 2013).~~

85 Tracer tests are commonly conducted in such aquifers to estimate transport parameters such as
86 effective porosity and dispersivity, to characterize subsurface heterogeneity, and to directly
87 delineate flow paths. ~~Testing involves injecting a tracer into the underground formation through an~~
88 ~~injection well, and then monitoring the tracer concentrations as a function of location and/or time at~~
89 ~~the surrounding observation well (breakthrough curve).~~

Formatted: Font color: Auto, English (U.K.)

Formatted: English (U.K.)

90 Transport parameters ~~such as porosity and dispersion coefficient~~ are estimated by fitting appropriate
91 tracer transport models to the breakthrough data, ~~(potrebbe essere eliminato troppo generico)~~

Formatted: Font color: Auto, English (U.K.)

Formatted: English (U.K.)

92 In this context, analytical models are frequently employed, especially for analyzing tests obtained
93 under controlled conditions, because they involve a small number of parameters and provide
94 physical insights into solute transport processes (Liu et al 2012).

95 The advection – dispersion equation (ADE) has been traditionally applied to model tracer transport
96 in fractures. However extensive evidence has shown that there exist two main features that cannot
97 be explained by the ADE: the early first arrival and the long tail of the observed BTCs curves.
98 (Neretnieks et al, 1982; Becker and Shapiro, 2000; Jiménez-Hornero et al. 2005; Bauget and Fourar,
99 2008).

100 Several other models have been used to fit the anomalous BTCs obtained in laboratory tracer tests
101 carried out in single fractures. Among those, the Mobile-Immobile (MIM) model (van Genuchten
102 and Wierenga, 1976), ~~which recognizes the existence of mobile and immobile domains for~~
103 ~~transport~~, has showed to provide better fits of BTC curves (Gao et al., 2009, Schumer et.al 2003,
104 Feehley et al, 2010).

105 In the well – controlled laboratory tracer tests carried out by Qian et al. (2011) a mobile– immobile
106 (MIM) model proved to fit both peak and tails of the observed BTCs better than the classical ADE
107 model.

108 Another powerful method to describe non – Fickian transport in fractured media is the continuous
109 time random walk (CTRW) approach (Berkowitz et al. 2006) which is based on the conceptual
110 picture of tracer particles undergoing a series of transitions of length s and time t .

111 Together with a master equation conserving solute mass, the random walk is developed into a
112 transport equation in partial differential equation form. The CTRW has been successfully applied
113 for describing non – Fickian transport in single fractures (Berkowitz et al.2001; Jiménez – Hornero
114 et al. 2005).

115 Bauget and Fourar (2008) investigated non – Fickian transport in a transparent replica of a real
116 single fracture. They employed three different models including ADE, CTRW, and a stratified
117 model to interpret the tracer experiments.

118 As expected, the solution derived from the ADE equation appears to be unable to model long-time
119 tailing ~~behavior~~behaviour. On the other hand, the CTRW and the stratified model were able to
120 describe non – Fickian dispersion. The parameters defined by these models are correlated to the
121 heterogeneities of the fracture.

122 Nowamooz et al., (2013) carried out experimental investigation and modeling analysis of tracer
123 transport in transparent replicas of two Vosges sandstone natural fractures.

Formatted: English (U.K.)

124 The obtained breakthrough curves were then interpreted using a stratified medium model that
125 incorporates a single parameter permeability distribution to account for fracture heterogeneity,
126 together with a CTRW model, as well as the classical ADE model.

Formatted: English (U.K.)

127 ~~The results confirmed poorly fitting breakthrough curves for ADE. The results indicated that the~~
128 ~~classical ADE is not appropriate for modeling early arrival and long time tailing.~~ In contrast, the
129 stratified model provides generally satisfactory matches to the data (even though it cannot explain
130 the long-time tailing adequately) while the CTRW model captures the full evolution of the long
131 tailing displayed by the breakthrough curves.

Formatted: English (U.K.)

132 Qian et al (2011) experimentally studied solute transport in a single fracture (SF) under non –
133 Darcian flow condition which was found to closely follow the Forchheimer equation.

134 They also investigated on the influence of the velocity contrast between the fracture wall and the
135 plane of symmetry on the dispersion process, which was called ‘boundary layer dispersion’ by
136 Koch and Brady (1985).

137 They affirmed that this phenomenon had to be considered if the thickness of the boundary layer was
138 greater than the roughness of the fracture. On the other hand, if the thickness of the boundary layer
139 was smaller than the roughness of the fractures, the recirculation zones inside the roughness cavities
140 rather than the boundary layer would be more relevant for the dispersion process, thus the hold – up
141 dispersion would become important. Since smooth parallel planes were used for constructing the SF
142 in their experiment, the fracture roughness and the hold – up dispersion were negligible.

Formatted: Space After: 0 pt

143 Bodin et al (2007) developed the SOLFRAC program, which performs fast simulations of solute
144 transport in complex 2D fracture networks using the Time Domain Random Walk (TDRW)
145 approach (Delay & Bodin, 2001) that makes use of a pipe network approximation. The code
146 accounts for advection and hydrodynamic dispersion in the channels, matrix diffusion, diffusion
147 into stagnant zones within the fracture planes, mass sharing at fracture intersections, and other
148 mechanisms such as sorption reactions and radioactive decay. Comparisons between numerical
149 results and analytical breakthrough curves for synthetic test problems have proven the accuracy of
150 the model.

151 Zafarani & Detwiler (2013) presented an alternate approach for efficiently simulating transport
152 through fracture intersections.

153 Rather than solving the two – dimensional Stokes equations, the model relies upon a simplified
154 velocity distribution within the fracture intersection, assuming local parabolic velocity profiles
155 within fractures entering and exiting the fracture intersection. Therefore, the solution of the two –
156 dimensional Stokes equations is unnecessary, which greatly reduces the computational complexity.

Formatted: Space After: 10 pt

157 The use of a time – domain approach to route particles through the fracture intersection in a single
158 step further reduces the number of required computations. The model accurately reproduces mixing
159 ratios predicted by high – resolution benchmark simulations.

160 ~~As most of previous investigations of flow and transport in fracture networks considered Darcian~~
161 ~~flow, and there are few controlled laboratory experiments on solute transport under non Darcian~~
162 ~~flow. Furthermore the behaviour of the solute transport in fracture networks under non – darcian~~
163 ~~flow conditions has been therefore poorly investigated. In the fracture networks different pathways~~
164 ~~can be identified through which solute is generally distributed in function of the energy spent by~~
165 ~~solute particles to cross the path. In this context the presence of nonlinear flow could plays an~~
166 ~~important role in the distribution of the solutes according to the different pathways. In fact the~~
167 ~~energy spent to cross the path should be proportional to the resistance to flow associated to the~~
168 ~~single pathway, which in nonlinear flow regime is not constant but depends on the flow rate. This~~
169 ~~means that changing the boundary conditions the resistance to flow varies and as a consequence the~~
170 ~~distribution of solute in the main and secondary pathways also changes giving rise to a different~~
171 ~~behaviour of solute transport.~~

172 ~~Most of previous investigations of flow and transport in fracture networks considered Darcian flow.~~
173 ~~and there are few controlled laboratory experiments on solute transport under non Darcian flow.~~

174 In previous studies by Cherubini et al (2012, 2013) the presence of nonlinear flow and non fickian
175 transport in a fractured rock formation has been analyzed at bench scale in laboratory tests.

176 The effects of nonlinearity in flow have been investigated by analyzing hydraulic tests on
177 an artificially created fractured limestone block of parallelepiped ($0.60 \times 0.40 \times 0.8 \text{ m}^3$) shape.

178 The flow tests regard the observation of the volumes of water passing through different paths across
179 the fractured sample. In particular, the inlet flow rate and the – for various hydraulic head
180 difference between the inlet and outlet ports – have been measured. The experimental results
181 have shown evidence of a non-Darcy relationship between flow rate and hydraulic head
182 differences, that is best described by a polynomial expression, Forchheimer’s law. Transition
183 from viscous dominant regime to inertial dominant regime has been detected. The experiments
184 have been compared with a 3d numerical model in order to evaluate the linear and non-linear terms
185 of Forchheimer equation for each paths.

186 Moreover, a tortuosity factor has been determined which is a measure of the deviation of each flow
187 path from the parallel plate model. A power law has been detected between the Forchheimer terms
188 and the tortuosity factor, which means that the latter influences flow dynamics. (va accennato anche
189 il discorso della tortuosità)

Formatted: English (U.K.)

Formatted: English (U.K.)

Formatted: Font color: Auto, English (U.K.)

Formatted: Font color: Auto, English (U.K.)

Formatted: Font color: Auto, English (U.K.)

Formatted: English (U.K.)

Formatted: English (U.K.)

Formatted: English (U.K.)

Formatted: English (U.K.)

Formatted: English (U.K.)

Formatted: English (U.K.)

Formatted: English (U.K.)

Formatted: English (U.K.)

Formatted: English (U.K.)

Formatted: English (U.K.)

Formatted: English (U.K.)

Formatted: Font color: Auto

Formatted: English (U.K.)

Formatted: Font color: Auto

Formatted: English (U.K.)

Formatted: English (U.K.)

Formatted: Font color: Auto

Formatted: English (U.K.)

Formatted: Font color: Auto, English (U.K.)

Formatted: English (U.K.)

190 ~~and the results of the experiments have been reported as specific flow rate vs. head gradient (Fig~~
191 ~~1)).~~

192 The non fickian nature of transport has been investigated by means of tracer tests that regard the
193 measurement of breakthrough curves for saline tracer pulse across a selected path varying the flow
194 rate.

195 ~~The experimental results have shown evidence of a non Darcy relationship between flow rate and~~
196 ~~hydraulic loss that is best described by Forchheimer's law. Transition from viscous dominant~~
197 ~~regime to inertial dominant regime has been detected.~~ The observed experimental breakthrough
198 curves of solute transport have proved to be better modeled by the 1d analytical solution of MIM
199 model approach which recognizes the existence of mobile and immobile domains for transport.

200 The carried out experiments show that there exists a pronounced mobile-immobile zone interaction
201 that cannot be neglected and that leads to a non-equilibrium behaviour of solute transport. The
202 existence of a non-Darcian flow regime has showed to influence the velocity field in that it gives
203 rise to a delay in solute migration with respect to the predicted value assuming linear flow.
204 furthermoreFurthermoreTherefore the presence of inertial effects has proved to enhance non-
205 equilibrium behaviour.

206 Instead, the presence of a transitional flow regime seems not to exert influence on the behaviour of
207 dispersion. The linear type relationship found between velocity and dispersion demonstrates that for
208 the range of imposed flow rates and for the selected path the geometrical dispersion dominates the
209 mixing processes along the fracture network.

210 The authors concluded that for the case study, where a fracture network is present, fracture
211 intersections interrupt the continuity of flow paths between single fractures and give rise to velocity
212 fluctuations that do not permit Taylor dispersion to "develop" and instead enhance geometrical
213 dispersion.

214
215 Herein, in order to give a more physical interpretation of the flow and transport behaviour, we build
216 on the work by Cherubini et al (2013) by interpreting the obtained experimental results of flow and
217 transport tests by means of the comparison of two conceptual models: the 1d single rate mobile –
218 immobile model (MIM) and the 2d Explicit Network Model (ENM). Differently from the former,
219 the latter expressly takes the fracture network geometry into account.

220
221 Starting from previous studies (Cherubini et al, 2012, 2013a), in order to give a physical
222 interpretation of the flow and transport behavior, in this work the experimental results of flow and
223 transport tests in a fractured block at bench scale are interpreted by means of two conceptual

Formatted: Font color: Auto
Formatted: English (U.K.)

Formatted: English (U.K.), Not Highlight
Formatted: English (U.K.)
Formatted: English (U.K.), Not Highlight
Formatted: English (U.K.)
Formatted: English (U.K.)
Formatted: English (U.K.)

models: the single rate mobile-immobile model (MIM) and the Explicit Network Model (ENM).
Differently from the former, the latter expressly takes the fracture network geometry into account.
The MIM approach is applied successfully in a broad variety of environmental context such as
rivers and streams with hypoeiric zone exchange, subsurface flow and transport in unsaturated and
saturated heterogeneous media, reactive solute transport etc.

When applied ~~to in~~ fractured media, the MIM approach does not explicitly take the fracture network
geometry into account, but it conceptualizes the shape of fractures as 1d one dimensional continuous
media in which the liquid phase is separated into flowing and stagnant regions. The convective
dispersive transport is restricted to the flowing region, and the solute exchange is described as a first
– order process.

Unlike MIM, the ENM model may allow to know the physical meaning of ~~the~~ flow and transport
phenomena (i.e the meaning of long – time ~~behavior~~behaviour of BTC curves that characterize
fractured media) and permits to obtain a more accurate estimation of flow and solute transport
parameters. In this model the fractures are represented as 1d – pipe elements and they form a 2d –
pipe network.

It is clear that ENM needs to address the problem of parameterization. In fact the transport
parameters of each individual fracture should be specified and this leads to more uncertainty in the
estimation.

Our overarching objective is therefore of investigating the performances and the reliabilities of
MIM and ENM approaches to describe conservative tracer transport in a fractured rock sample.

The present paper aims to investigate the performance and the reliabilities of MIM and ENM
approaches. In particular way the present paper focuses the attention on the effects of non-linear
flow regime on different features ~~which that~~ depict the conservative solute transport in a fractured
network ~~such as including~~ mean travel time, dispersion, dual porosity behaviour, distribution of
solute into ~~the~~ different pathways.

The aim of this work is therefore to compare the performances and the reliabilities of MIM and
ENM approaches in nonlinear flow regime to describe conservative tracer transport in a fractured
rock sample. In particular manner the present paper aims to investigate (specificare nel dettaglio
gli obiettivi del paper)

Formatted: English (U.K.)

Formatted: English (U.K.)

Formatted: Font color: Text 1, English (U.K.),
Not Highlight

Formatted: English (U.K.)

Formatted: Font color: Text 1, English (U.K.),
Not Highlight

Formatted: Font color: Text 1, English (U.K.)

Formatted: Font color: Text 1, English (U.K.)

Formatted: English (U.K.)

Formatted: Font color: Text 1, English (U.K.)

Formatted: English (U.K.)

Formatted: Font color: Text 1, English (U.K.)

Formatted: Font color: Red, English (U.K.),
Highlight

Formatted: English (U.K.)

253 **Theoretical background**

254 **Nonlinear flow**

255 In the literature different laws are reported that account for the nonlinear relation ship between
256 velocity and pressure gradient.

257 A cubic extension of Darcy's law that describes pressure loss versus flow rate for low flow rates is
258 the weak inertia equation:

259
$$-\frac{dp}{dx} = \frac{\mu}{k} \cdot v + \frac{\gamma \rho^2}{\mu} \cdot v^3$$
 (111)

260 Where p (ML⁻¹T⁻²) is the pressure, k (L²) is the permeability, μ (ML⁻¹T⁻¹) is the viscosity, ρ (ML⁻³)
261 is the density, v (LT⁻¹) is the velocity and γ (L) is called the weak inertia factor.

262 In case of higher Reynolds numbers (Re >> 1) the pressure losses pass from a weak inertial to a
263 strong inertial regime, described by the Forchheimer equation (Forchheimer, 1901), given by:

264
$$-\frac{dp}{dx} = \frac{\mu}{k} \cdot v + \rho \beta \cdot v^2$$
 (222)

265 Where β (L⁻¹) is called the inertial resistance coefficient, or non – Darcy coefficient.

266 Forchheimer law can be written in terms of hydraulic head:

267
$$-\frac{dh}{dx} = a' \cdot v + b' \cdot v^2$$
 (333)

268 Where a' (TL⁻¹) and b' (TL⁻²) are the linear and inertial coefficient respectively equal to:

269
$$a' = \frac{\mu}{\rho g k}; b' = \frac{\beta}{g}$$
 (444)

270 In the same way the relationship between flow rate Q (L³T⁻¹) and hydraulic head gradient can be
271 written as:

272 ~~$$-\nabla h = a \cdot Q + b \cdot Q^2$$~~
$$-\frac{dh}{dx} = a \cdot Q + b \cdot Q^2$$
 (555)

273 Where a (TL⁻³) and b (T²L⁻⁶) are related to a' and b' :

Formatted: English (U.K.)

Formatted: English (U.K.)

Formatted: English (U.K.)

Formatted: English (U.K.)

Formatted: English (U.K.)

Formatted: English (U.K.)

Formatted: English (U.K.)

Formatted: English (U.K.)

Formatted: English (U.K.)

Formatted: English (U.K.)

Formatted: English (U.K.)

Formatted: English (U.K.)

Formatted: English (U.K.)

Formatted: English (U.K.)

Formatted: English (U.K.)

Formatted: English (U.K.)

Formatted: English (U.K.)

Formatted: English (U.K.)

Formatted: English (U.K.)

Formatted: English (U.K.)

Field Code Changed

Formatted: English (U.K.)

Formatted: English (U.K.)

Formatted: English (U.K.)

274

$$a = \frac{a'}{\omega_{eq}}; b = \frac{b'}{\omega_{eq}}$$

(666)

Formatted: English (U.K.)
Formatted: English (U.K.)
Formatted: English (U.K.)

275

Where ω_{eq} (L^2) represents the [equivalent](#) cross sectional area of fracture.

Formatted: English (U.K.)
Formatted: English (U.K.)

276

Mobile Immobile Model

277

The mathematical formulation of the MIM for non - reactive solute transport is usually given as

278

follows:

279

$$\frac{\partial c_m}{\partial t} = D \frac{\partial^2 c_m}{\partial x^2} - v \frac{\partial c_m}{\partial x} - \alpha (c_m - c_{im})$$
$$\beta \frac{\partial c_{im}}{\partial t} = \alpha (c_m - c_{im})$$

(777)

Formatted: English (U.K.)
Formatted: English (U.K.)
Formatted: English (U.K.)

280

Where t (T) is the time, x (L) is the spatial coordinate along the direction of the flow, c_m and c_{im}

281

(ML^{-3}) are the cross - sectional averaged solute concentrations respectively in the mobile and

282

immobile domain, v (LT^{-1}) is the average flow velocity and D (L^2T^{-1}) is the dispersion coefficient, α

283

(T^{-1}) is the mass exchange coefficient, β [-] is the mobile water fraction. For a non – reactive solute

284

β is equivalent to the ratio between the immobile and mobile cross – sectional area (-).

Formatted: English (U.K.)
Formatted: English (U.K.)

285

The solution of system Equation (7) describing one – dimensional (1d) non – reactive solute

286

transport in an infinite domain for instantaneous pulse of solute injected at time zero at the origin is

287

given by (Goltz & Roberts, 1986):

288

$$c_m(x,t) = e^{-\alpha t} c_0(x,t) + \alpha \int_0^t H(t,\tau) c_0(x,\tau) d\tau$$

(888)

Formatted: English (U.K.)
Formatted: English (U.K.)
Formatted: English (U.K.)

289

[Where](#) c_0 represents the analytical solution for the classical advection – dispersion equation (Crank,

290

1956):

Formatted: English (U.K.)

291

$$c_0(x,t) = \frac{M_0}{\omega_{eq} \sqrt{\pi D t}} e^{-\frac{(x-vt)^2}{4Dt}}$$

(999)

Formatted: English (U.K.)
Formatted: English (U.K.)
Formatted: English (U.K.)

292

Where M_0 (M) is the mass of the tracer injected instantaneously at time zero at the origin of the

293

domain. The term $H(t,\tau)$ presents the following expression:

Formatted: English (U.K.)

294

$$H(t,\tau) = e^{-\frac{\alpha}{\beta}(t-\tau)-\alpha\tau} \frac{\tau I_1\left(\frac{2\alpha}{\beta}\sqrt{\beta(t-\tau)\tau}\right)}{\sqrt{\beta(t-\tau)\tau}}$$

(101010)

Formatted: English (U.K.)
Formatted: English (U.K.)
Formatted: English (U.K.)

320 Generally in a 2d fracture network, the single fracture can be set in series and/or in parallel.

321 In particular the total resistance to flow of a network in which the fractures are arranged in a chain
322 is found by simply adding up the resistance values of the individual fractures.

323 In a parallel network the flow breaks up by flowing through each parallel branch and re –
324 combining when the branches meet again. The total resistance to flow is found by adding up the
325 reciprocals of the resistance values and then taking the reciprocal of the total. The flow rate crossing
326 the generic fracture j belonging to parallel circuits Q_j can be obtained as:

327
$$Q_j = \sum Q \frac{1}{R_j} \left(\sum_{i=1}^n \frac{1}{R_i} \right)^{-1}$$
 (141414)

Formatted: English (U.K.)

Formatted: English (U.K.)

Formatted: English (U.K.)

328 Where $\sum Q$ (LT³) is the sum of the discharge flow evaluated for the fracture intersection located
329 in correspondence of the inlet bond of j fractures, whereas the term in brackets represents the
330 probability of water distribution of j fracture P_{Qj} .

Formatted: English (U.K.)

331 The BTC curves at the outlet of the network $c_{out}(t)$ (ML⁻³), for an instantaneous injection, can be
332 obtained as the summation of BTCs of each elementary path in the network. The latter can be
333 expressed as the convolution product of the probability density functions of residence times in each
334 individual fracture belonging to the elementary path. Using the convolution theorem, $c_{out}(t)$ can be
335 expressed as:

Formatted: English (U.K.)

Formatted: English (U.K.)

336
$$c_{out}(t) = \frac{M_0}{Q_0} F^{-1} \left[\sum_{i=1}^{N_{ep}} \prod_{j=1}^{n_{fi}} P_{c,j} F(s_j(l_j, t)) \right]$$
 (151515)

Formatted: English (U.K.)

Formatted: English (U.K.)

Formatted: English (U.K.)

337 Where M_0 (M) is the injected mass of solute, F is the Fourier transform operator, N_{ep} is the number
338 of the elementary paths, n_{fi} is the number of fractures in i elementary path, $P_{c,j}$ and $s_j(l_j, t)$ (T⁻¹)
339 represents the fraction of solute crossing the single fracture and the probability density function of
340 residence time respectively.

Formatted: English (U.K.)

Formatted: English (U.K.)

341 $P_{c,j}$ can be estimated as the probability of the particle transition in correspondence of the inlet bond
342 of each individual single fracture. The rules for particle transition through fracture intersections play
343 an important role in mass transport. In literature several models have been developed and tested in
344 order to represent the mass transfer within fracture intersections. The simplest rule is represented by

Formatted: English (U.K.)

345 the “perfect mixing model” in which the mass sharing is proportional to the relative discharge flow
346 rates.

347 The perfect mixing model assumes that the probability of particle transition of the fraction of solute
348 crossing the single fracture can be written as:

349
$$P_{c,j} = \frac{Q_j}{\sum Q}$$
 (161616)

350 Where Q_j represents the flow rate in the single j fracture. Note that if assuming valid the perfect
351 mixing model P_{Qj} is equal to P_{cj} .

352 It is clear that in order to know $s_j(l_j, t)$ the transport model and consequently the transport
353 parameters of each single fracture need to be defined. $s_j(l_j, t)$ can be evaluated in a simple way
354 using the 1D analytical solution of the Advection Dispersion Equation model (ADE) for pulse
355 input:

356
$$s_j(l_j, t) = \frac{Q_j}{\omega_{eq,j} \sqrt{\pi D_j t}} e^{-\frac{(l_j - v_j t)^2}{4 D_j t}}$$
 (171717)

357 in which the velocity v_j and dispersion D_j relating to the generic j fracture can be estimated
358 through the following expression:

359
$$v_j = \frac{Q_j}{\omega_{eq,j}}$$
 (181818)

360
$$D_j = \alpha_{L,j} v_j$$
 (191919)

361 Where $\omega_{eq,j}$ and $\alpha_{L,j}$ are the equivalent crossing area and the dispersion coefficient of j fracture
362 respectively.

363 The ENM is defined by six parameters regarding each single fracture ($a, b, P_Q, \omega_{eq}, \alpha_L$ and P_c).

Formatted: English (U.K.)

Formatted: English (U.K.)

Formatted: English (U.K.)

Formatted: English (U.K.)

Formatted: English (U.K.)

Formatted: English (U.K.)

Formatted: English (U.K.)

Formatted: English (U.K.)

Formatted: English (U.K.)

Formatted: English (U.K.)

Formatted: English (U.K.)

Formatted: English (U.K.)

Formatted: English (U.K.)

Formatted: English (U.K.)

Formatted: English (U.K.)

Formatted: English (U.K.)

Formatted: English (U.K.)

Formatted: English (U.K.)

Formatted: English (U.K.)

Formatted: English (U.K.)

364 **Material and methods**

365 **Experimental setup**

366 ~~The experiments have been performed on a limestone block with parallelepiped shape~~
367 ~~(0.6×0.4×0.08 m³) recovered from the ‘Calcere di Altamura’ formation which is located in Apulia~~
368 ~~region in southeastern Italy (Cherubini et al., 2012).~~

369 ~~The experimental setup is detailed in Cherubini et al. (2012) and Cherubini et al. (2013a) and its~~
370 ~~schematic diagram is shown in Fig 1.~~

371 **Flow and tracer tests**

372 ~~The experimental setup has been already extensively discussed in Cherubini et al. (2013), however~~
373 ~~for the completeness in this section a summary is reported—a summary.~~ The analysis of flow
374 dynamics through the selected path (Fig 2) regards the observation of water flow from the upstream
375 tank to the flow cell with a circular cross-section of 0.1963 m² and 1.28×10⁻⁴ m² respectively.

376 Initially at time t_0 , the valves ‘a’ and ‘b’ are closed and the hydrostatic head in the flow cell is equal
377 to h_0 . The experiment begins with the opening of the valve ‘a’ which is reclosed when the hydraulic
378 head in the flow cell is equal to h_l . Finally the hydraulic head in the flow cell is reported to h_0
379 through the opening of the valve ‘b’. The experiment procedure is repeated changing the hydraulic
380 head of the upstream tank h_c . The time $\Delta t = (t_1 - t_0)$ required to fill the flow cell from h_0 to h_l has
381 been registered.

382 Given that the capacity of the upstream tank is much higher than that of the flow cell it is
383 reasonable to assume that during the experiments the level of the upstream tank (h_c) remains
384 constant. Under this hypothesis the flow inside the system is governed by the equation:

385
$$S_l \frac{dh}{dt} = \Gamma(\Delta h)(h_c - h) \quad (202020)$$

386 Where S_l (L²) and h (L) are respectively the section area and the hydraulic head of the flow cell; h_c
387 (L) is the hydraulic head of upstream tank, $\Gamma(\Delta h)$ represents the hydraulic conductance term
388 representative of both hydraulic circuit and the selected path.

389 The average flow rate \bar{Q} can be estimated by means of the volumetric method:

390
$$\bar{Q} = \frac{S_l}{t_1 - t_0} (h_1 - h_0) \quad (212121)$$

Formatted: Font color: Text 1, English (U.K.)

Formatted: English (U.K.)

Formatted: Font color: Blue, English (U.K.)

Formatted: English (U.K.)

Formatted: English (U.K.)

Formatted: English (U.K.)

Formatted: English (U.K.)

Formatted: English (U.K.)

Formatted: English (U.K.)

Formatted: English (U.K.)

Formatted: English (U.K.)

Formatted: English (U.K.)

Formatted: English (U.K.)

Formatted: English (U.K.)

Formatted: English (U.K.)

Formatted: English (U.K.)

Formatted: English (U.K.)

Formatted: English (U.K.)

Formatted: English (U.K.)

391 Whereas the average hydraulic head difference $\overline{\Delta h}$ is given by: Formatted: English (U.K.)

392
$$\overline{\Delta h} = h_c - \frac{h_0 + h_1}{2}$$
 (222222) Formatted: English (U.K.)
Formatted: English (U.K.)
Formatted: English (U.K.)

393 In correspondence of the average flow rate and head difference is it possible to evaluate the average
394 hydraulic conductance as:

395
$$\bar{\Gamma}(\Delta h) = \frac{S_1}{t_1 - t_0} \ln \left(\frac{h_0 - h_c}{h_1 - h_c} \right)$$
 (232323) Formatted: English (U.K.)
Formatted: English (U.K.)
Formatted: English (U.K.)

396 The inverse of $\bar{\Gamma}(\Delta h)$ represents the average resistance to flow $\bar{R}(\bar{Q})$. Formatted: English (U.K.)
Formatted: English (U.K.)

397 **Tracer tests**

398 The study of solute transport dynamics through the selected path has been carried out by means of a
399 tracer test using sodium chloride. Initially a hydraulic head difference between the upstream tank
400 and downstream tank is imposed. At $t = 0$ the valve 'a' is closed and the hydrostatic head inside the
401 block is equal to the downstream tank. At $t = 10$ s the valve 'a' is opened while at time $t = 60$ s a
402 mass of solute equal to 5×10^{-4} kg is injected into the inlet port through a syringe. The source release
403 time (1 s) is very small therefore the instantaneous source assumption can be considered valid.

404 In correspondence of the flow cell in which the multi - parametric probe is located it is possible to
405 measure the tracer breakthrough curve and the hydraulic head; in the meanwhile the flow rate
406 entering the system is measured by means of an ultrasonic velocimeter. For different flow rates a
407 BTC curve can be recorded at the outlet port.

408 Time moment analysis has been applied in order to characterize the BTC curves in terms of mean
409 breakthrough time, degree of spread and asymmetry.

410 The mean residence time t_m is given by:

411
$$t_m = \frac{\int_0^{\infty} t^n c(t) dt}{\int_0^{\infty} c(t) dt}$$
 (242424) Formatted: English (U.K.)
Formatted: English (U.K.)
Formatted: English (U.K.)

412 The n^{th} normalized central moment of distribution of solute concentration versus time is defined as:

413

$$\mu_n = \frac{\int_0^{\infty} [t - t_m]^n c(t) dt}{\int_0^{\infty} c(t) dt}$$

(252525)

Formatted: English (U.K.)

Formatted: English (U.K.)

Formatted: English (U.K.)

414

The second moment μ_2 represents the degree of spread relative to t_m whereas the degree of

Formatted: English (U.K.)

415

asymmetry measured by the skewness coefficient is defined as:

416

$$S = \mu_3 / \mu_2^{3/2}$$

(262626)

Formatted: English (U.K.)

Formatted: English (U.K.)

Formatted: English (U.K.)

417

Discussion

418

Estimation of flow model parameters

419

The flow field in each single fracture of the network can be solved in analytical way by means of Kirchhoff laws. In Figure 2 is represented the 2d – pipe network conceptualization.

421

The resistance to flow of each single fracture is described by the Equation (12). The Forchheimer parameters are assumed constant for the whole fracture network.

423

The application of the Kirchhoff's first law at the node 3 can be written as:

424

$$Q_0 - Q_1 - Q_2 = 0$$

(272727)

Formatted: English (U.K.)

Formatted: English (U.K.)

Formatted: English (U.K.)

425

Whereas the application of the Kirchhoff's second law at the loop 3 – 4 – 5 – 6 can be written as:

426

$$R_6(Q_1)Q_1 - (R_3(Q_2) + R_4(Q_2) + R_5(Q_2))Q_2 = 0$$

(282828)

Formatted: English (U.K.)

Formatted: English (U.K.)

Formatted: English (U.K.)

427

Substituting Equation (278) into Equation (289) the iterative equation of flow rate Q_I can be obtained:

428

429

$$Q_1^{k+1} = Q_0 \left[\frac{R_3(Q_0 - Q_1^k) + R_4(Q_0 - Q_1^k) + R_5(Q_0 - Q_1^k)}{R_3(Q_0 - Q_1^k) + R_4(Q_0 - Q_1^k) + R_5(Q_0 - Q_1^k) + R_6(Q_1^k)} \right]$$

(292929)

Formatted: English (U.K.)

Formatted: English (U.K.)

Formatted: English (U.K.)

430

The Forchheimer parameters representative of whole fracture network can be derived matching the average resistance to flow derived experimentally with the resistance to flow evaluated for the whole network:

431

432

433

$$\bar{R}(\bar{Q}) = R_1(Q_0) + R_2(Q_0) + \left(\frac{1}{R_6(Q_1)} + \frac{1}{R_3(Q_2) + R_4(Q_2) + R_5(Q_2)} \right)^{-1} + R_7(Q_0) + R_8(Q_0) + R_9(Q_0)$$

(303030)

Formatted: English (U.K.)

Formatted: English (U.K.)

Formatted: English (U.K.)

Figure 3 shows the fitting of observed resistance to flow determined by the inverse of Equation (234) and the theoretical resistance to flow (Equation 304). The linear and nonlinear terms of Forchheimer model in Equation (12) have been estimated and they are respectively equal to $a = 7.345 \times 10^4 \text{ sm}^{-3}$ and $b = 11.65 \times 10^9 \text{ s}^2 \text{ m}^{-6}$. It is evident that the 2d - pipe network model closely matches the experimental results ($r^2 = 0.9913$). Flow characteristics can be studied through the analysis of Forchheimer number F_0 which represents the ratio of nonlinear to linear hydraulic gradient contribution:

$$F_0 = \frac{bQ}{a} \quad (313134)$$

Inertial forces dominate over viscous ones at the critical Forchheimer number ($F_0=1$) corresponding in our case to a flow rate equal to $Q_{crit} = 6.30 \times 10^{-6} \text{ m}^3/\text{s}$, which is coherent with the results obtained in the previous study (Cherubini et al., 2013a).

The term in square brackets in Equation (30) represents the probability of water distribution P_Q evaluated for the branch 6. Note that it is not constant but it depends on the flow rate crossing the parallel branch. Figure 4 shows P_Q as function of Q_0 . The probability of water distribution decreases as the injection flow rate increases. This means that when the injection flow rate increases the resistance to flow of the branch 6 increases faster than the resistance to flow of the branch 3 – 4 – 5 and therefore the solute choses the secondary pathway.

Fitting of breakthrough curves and interpretation of estimated transport model parameters

Several tests have been conducted in order to observe solute transport behaviour varying the injection flow rate in the range $1.20 \times 10^{-6} - 9.34 \times 10^{-6} \text{ m}^3 \text{ s}^{-1}$. For each experimental BTCs the mean travel time t_m and the coefficient of Skewness S have been estimated.

Figure 5 shows t_m as function of Q_0 . Travel time decreases more slowly for high flow rates. In particular a change of slope is evident in correspondence of the injection flow rate equal to $4 \times 10^{-6} \text{ m}^3 \text{ s}^{-1}$ (Cherubini et al., 2013a), which evidences a delay of solute transport for high flow rates, which means the setting up of a transitional flow regime; the diagram of velocity profile is flattened because of inertial forces prevailing on viscous one, as already showed by Cherubini et al (2013a). The presence of a transitional flow regime leads to a delay on solute transport with respect to the values that can be obtained under the assumption of a linear flow field. Note that this behaviour occurs before of Q_{crit} .

Formatted: English (U.K.)

Formatted: English (U.K.)

Formatted: English (U.K.)

Formatted: English (U.K.)

464 The skewness coefficient does not exhibit a trend upon varying the injection flow rate, but its mean
465 value is equal to 2.018. A positive value of skewness indicates that BTCs are asymmetric with early
466 first arrival and long tail. This behavior seems not to be dependent on the presence of the
467 transitional regime.

468 The measured breakthrough curves for different flow rates have been individually fitted by the
469 MIM $\left(v/L, D/L^2, \alpha, \beta\right)$ and ENM $\left(\omega_{eq}, \alpha_L, P_Q, P_C\right)$ models.

470 In particular for the ENM model the parameters ω_{eq} (equivalent area) and α_L are representative of
471 all fracture network, whereas the parameters P_Q and P_C are associated only to the parallel branches.
472 For the considered fracture network the Equation (156) becomes:

473
$$c_{out} = \frac{M_0}{Q_0} F^{-1} \left[\frac{P_c \cdot F(s_1) \cdot F(s_2) \cdot F(s_6) \cdot F(s_7) \cdot F(s_8) \cdot F(s_9) +}{+ (1 - P_c) \cdot F(s_1) \cdot F(s_2) \cdot F(s_3) \cdot F(s_4) \cdot F(s_5) \cdot F(s_7) \cdot F(s_8) \cdot F(s_9)} \right] \quad (323232)$$

474 The velocity and dispersion that characterize the probability density function s are related to the
475 flow rate that crosses each branch by Equation (189) and Equation (1920). This one is equal to the
476 injection flow rate Q_0 except for branch 6 and branches 3 – 4 – 5 for which it is equal to $Q = P_Q Q_0$
477 and $Q = (1 - P_Q) Q_0$ respectively.

478 Furthermore three parameter configurations have been tested for the ENM model. The
479 configurations are distinguished on the basis of the number of fitting parameters and assumptions
480 made on P_C and P_Q parameters. The first configuration named ENM2 has two fitting parameters
481 ω_{eq} and α_L . In this configuration P_C is imposed equal to P_Q and is derived as the square brackets
482 term in Equation (29). estimated by the flow tests described in previous sections.

483 The second configuration named ENM3 has three fitting parameters ω_{eq} and α_L and P_C (P_Q). In this
484 configuration is it still true that P_C is still equal to P_Q but they and both of them are
485 evaluated ~~estimated~~ by the interpretation of BTC curves.

486 In the third configuration named ENM4 all four parameters $\left(\omega_{eq}, \alpha_L, P_Q, P_C\right)$ are estimated
487 determined through the fitting of BTCs.

Formatted: English (U.K.)

Formatted: English (U.K.)

Formatted: English (U.K.)

Formatted: English (U.K.)

Formatted: English (U.K.)

Formatted: English (U.K.)

Formatted: English (U.K.)

Formatted: English (U.K.)

Formatted: English (U.K.)

Formatted: English (U.K.)

Formatted: English (U.K.)

Formatted: English (U.K.)

Formatted: English (U.K.)

Formatted: English (U.K.)

Formatted: English (U.K.)

Formatted: English (U.K.)

Formatted: English (U.K.)

Formatted: English (U.K.)

Formatted: English (U.K.)

Formatted: English (U.K.)

Formatted: English (U.K.)

Formatted: English (U.K.)

Formatted: English (U.K.), Not Highlight

Formatted: English (U.K.)

Formatted: English (U.K.)

Formatted: English (U.K.)

Formatted: English (U.K.)

Formatted: English (U.K.)

Formatted: English (U.K.)

Formatted: English (U.K.)

Formatted: English (U.K.)

Formatted: English (U.K.)

Formatted: English (U.K.)

Formatted: English (U.K.)

Formatted: English (U.K.)

Formatted: English (U.K.)

Formatted: English (U.K.)

Formatted: English (U.K.)

Formatted: English (U.K.)

Formatted: English (U.K.)

Formatted: English (U.K.)

Formatted: English (U.K.)

Formatted: English (U.K.)

Formatted: English (U.K.)

Formatted: English (U.K.)

Formatted: English (U.K.)

Formatted: English (U.K.)

Formatted: English (U.K.)

Formatted: English (U.K.)

Formatted: English (U.K.)

Formatted: English (U.K.)

488 To compare all the considered models, both the determination coefficient (r^2) and the root mean
 489 square error (RMSE) were used as criteria to determine the goodness of the fitting, which can be
 490 expressed as:

491
$$r^2 = 1 - \frac{\sum_{i=1}^N (C_{i,o} - C_{i,e})^2}{\sum_{i=1}^N (C_{i,o} - \bar{C}_{i,o})^2}$$
 (333333)

Formatted: English (U.K.)
 Formatted: English (U.K.)
 Formatted: English (U.K.)

492
$$RMSE = \sqrt{\frac{1}{N} \sum_{i=1}^N (C_{i,o} - C_{i,e})^2}$$
 (343434)

Formatted: English (U.K.)
 Formatted: English (U.K.)
 Formatted: English (U.K.)

493 Where N is the number of observations, $C_{i,e}$ is the estimated concentration, $C_{i,o}$ is the observed
 494 concentration and, $\bar{C}_{i,o}$ represents the mean value of $C_{i,o}$.

Formatted: English (U.K.)
 Formatted: English (U.K.)

495 Tables 1, 2, 3 and 4 show the estimated values of parameters, root mean square error RMSE and the
 496 determination coefficient r^2 for all the considered models varying the inlet flow rate Q_0 .

497 Figure 6 shows the fitting results of BTC curves for different injection flow rates.

498 For higher flow rates (7.07×10^{-6} and 4.80×10^{-6} m³/s) the fitting is poorer than for lower flow rates
 499 (3.21×10^{-6} and 1.96×10^{-6} m³/s). However, all models provide a satisfactory fitting. The ENM4
 500 model provides the highest values of r^2 varying in the range 0.9921 – 1.000 and the smallest values
 501 of RMSE in the range 0.0033 – 0.0252. This is expected for two reasons. First this model has more
 502 fitting parameters than ENM2 and ENM3, thus it is more flexible. Second, compared to MIM
 503 model, it takes explicitly into account the presence of the secondary path.

504 The MIM model considers the existence of immobile and mobile domains and a rate – limited mass
 505 transfer between these two domains. In the present context this conceptualization can be a weak
 506 assumption especially for high flow rates when the importance of secondary path increases.
 507 However the fitting of BTCs shows that MIM model remains valid as it proves to describe the
 508 observed curves quite well.

509 The extent of solute mixing can be assessed from the analysis of MIM first-order mass transfer
 510 coefficient α and the fraction of mobile water β .

Formatted: English (U.K.), Not Highlight

511 ~~Although somewhat scattered, the mass transfer coefficient of MIM model tends to increase with~~
 512 ~~pore water velocity.~~ Several authors have observed the variation of the mass-transfer coefficient
 513 between mobile and immobile water regions with pore-water velocity (van Genuchten and

Formatted: Font: Italic, English (U.K.), Not Highlight

Formatted: English (U.K.), Not Highlight

Formatted: Font: Italic, English (U.K.), Not Highlight

Formatted: English (U.K.), Not Highlight

Formatted: English (U.K.)

Wierenga, 1977; Nkedi-Kizza et al., 1984; De Smedt and Wierenga, 1984; De Smedt et al., 1986; Schulin et al., 1987). The increase in α with increasing water velocity is attributed to higher mixing in the mobile phase at high pore water velocities (De Smedt and Wierenga, 1984) or to shorter diffusion path lengths as a result of a decrease in the amount of immobile water (van Genuchten and Wierenga, 1977).

Formatted: Font: Italic, English (U.K.)

Formatted: English (U.K.)

~~In the study, the increase in α with increasing water velocity is attributable to nonlinear flow that enhance the exchange between the main and secondary flow paths. Therefore the mass transfer coefficient increases as the importance of secondary path over the main path increases.~~

Formatted: English (U.K.)

Formatted: English (U.K.)

~~The extent of solute mixing can also be assessed from the analysis of MIM mobile water fraction parameter β . In our study the fraction of mobile water assumes a mean representative value of 0.56 meaning that the 0.56% of the fracture network soil is involved in advective transport. As concerns β , various authors have observed different behaviour of the mobile water fraction parameter β . Gaudet et al. (1977) reported increasing mobile water content with increasing pore water velocity. However, studies have also found that β appears to be constant with varying pore-water velocity (Nkedi-kizza et al. 1983). However, lower β values can be attributed to faster initial movement of the solute as it travels through a decreasing number of faster flow paths. As a result, some authors have related β values to the initial arrival of the solute. In fact, Gaudet et al. (1977) and Selim and Ma (1995) observed that the mobile water fraction parameter affects the time of initial appearance of the solute.~~

Formatted: English (U.K.)

Formatted: English (U.K.)

Formatted: Font: Italic, English (U.K.)

Formatted: English (U.K.)

Formatted: English (U.K.)

Formatted: English (U.K.)

Formatted: Font: Italic, English (U.K.)

Formatted: English (U.K.)

Formatted: Font: Italic, English (U.K.)

Formatted: English (U.K.)

Formatted: Font: Italic, English (U.K.)

Formatted: English (U.K.)

~~In general, the initial breakthrough time increases as β increases (Gao et al., 2009) which can also be evidenced from Fig 6. For lower flow rates the initial arrival time is higher than for higher flow rates. As the fraction of mobile water increases, the breakthrough curves are shifted to longer times because the solute is being transported through larger and larger fractions of the fracture volume. In the limiting case that the fraction of mobile water reaches one, the MIM reduces to the equilibrium ADE (no immobile water) (Mulla & Strock, 2008).~~

Formatted: Font: Italic, English (U.K.)

Formatted: English (U.K.)

~~The evidence of dual porosity behaviour on solute transport is clearly shown by the analysis of the two MIM parameters; the ratio of mobile and immobile area β and the mass exchange coefficient α shown in Figure 7 as a function of velocity.~~

Formatted: Space After: 0 pt

Formatted: English (U.K.)

Formatted: English (U.K.)

Formatted: English (U.K.)

Formatted: English (U.K.)

Formatted: English (U.K.)

Formatted: English (U.K.), Not Highlight

Formatted: English (U.K.)

Formatted: English (U.K.)

Formatted: English (U.K.)

Formatted: English (U.K.)

~~A different behaviour of these two coefficients to varying the injection flow rate is observed in the present study. At Darcian-like flow conditions the mass exchange coefficient remains constant, whereas the ratio of mobile and immobile area decreases as velocity increases. When nonlinear flow starts to become dominant a different behaviour is observed: α increases in a potential way, whereas β assumes a weakly growing trend as velocity increases with a mean value equal to 0.56.~~

Formatted: English (U.K.)

Formatted: English (U.K.)

Formatted: English (U.K.)

547 In order to better explain this behaviour, the transport time (reciprocal of normalized velocity) and
548 the exchange time (reciprocal of the exchange term) varying the flow rate for the MIM model are
549 showed in Figure 8. In analogous way in Figure 9 is showed the comparison between the mean
550 travel time for the main path and the secondary path varying the injection flow rate for the ENM4
551 model.

Formatted: English (U.K.)
Formatted: English (U.K.)
Formatted: English (U.K.)
Formatted: English (U.K.), Not Highlight
Formatted: English (U.K.)

552 For the MIM model at high flow rates the exchange time joins the transport time; analogously for
553 the ENM4 as the flow rate increases the secondary path reaches the main path in terms of mean
554 travel time. This analogy between MIM and ENM enhances the concept that the mass transfer
555 coefficient is dependent on flow velocity.

556 In Darcian-like flow conditions the main path is dominant on the secondary path. The latter can be
557 considered as an immobile zone. In this condition the fracture network behaves as a single fracture
558 and the observed dual porosity behaviour can be attributable only to the fracture – matrix
559 interactions of the main path.

Formatted: English (U.K.)
Formatted: English (U.K.)
Formatted: English (U.K.)

560 For higher velocities, a higher contact area between the mobile and immobile region is evidenced,
561 enhancing solute mixing between these two regions (Gao et al. 2009). The increase in α with
562 increasing water velocity is therefore attributable to nonlinear flow that enhances the exchange
563 between the main and secondary flow paths. Increasing the injection flow rate the importance of the
564 secondary path grows and the latter cannot be considered as an immobile zone, as a consequence
565 the dual porosity behaviour becomes stronger.

Formatted: English (U.K.), Not Highlight
Formatted: English (U.K.), Not Highlight
Formatted: Font: (Default) Times New Roman, English (U.K.), Not Highlight
Formatted: English (U.K.)

566 ~~Various authors have observed different behavior of the mobile water fraction parameter β_A . Gaudet~~
567 ~~et al. (1977) reported increasing mobile water content with increasing pore water velocity.~~
568 ~~However, studies have also found that β_A appears to be constant with varying pore water velocity~~
569 ~~(Nkedi kizza et al. 1983). With the increase of mobile water fraction, the contact areas between the~~
570 ~~mobile and immobile regions increase, enhancing solute mixing between these two regions (Gao et~~
571 ~~al., 2009). However, lower β_A values can be attributed to faster initial movement of the solute as it~~
572 ~~travels through a decreasing number of faster flow paths. As a result, some authors have related β_A~~
573 ~~values to the initial arrival of the solute. In fact, Gaudet et al. (1977) and Selim and Ma (1995)~~
574 ~~observed that the mobile water fraction parameter affects the time of initial appearance of the~~
575 ~~solute.~~

Formatted: English (U.K.)
Formatted: English (U.K.)
Formatted: English (U.K.)
Formatted: English (U.K.)
Formatted: English (U.K.)
Formatted: English (U.K.)
Formatted: English (U.K.)
Formatted: English (U.K.)

576 In general, the initial breakthrough time increases as β_A increases (Gao et al., 2009) which can also
577 be evidenced from Fig 6. For lower flow rates the initial arrival time is higher than for higher flow
578 rates. As the fraction of mobile water increases, the breakthrough curves are shifted to longer times

Formatted: English (U.K.)
Formatted: English (U.K.)

579 because the solute is being transported through larger and larger fractions of the fracture soil
580 volume. In the limiting case that the fraction of mobile water reaches one, the MIM reduces to the
581 equilibrium ADE (no immobile water) (Mulla & Strock, 2008).

582 As showed in figure 10.7 and 11.8 $\frac{P_c}{P_0}$ as function of Q_0 evaluated by means the fitting of
583 BTCs by ENM3 and ENM4 models presents a different trend respect to $\frac{P_c}{P_0}$
584 determined by means of flow tests. $\frac{P_c}{P_0}$ evaluated by transport tests decreases more
585 rapidly than $\frac{P_c}{P_0}$ determined by flow tests (Figure 10.7). In the ENM4 model $\frac{P_c}{P_0}$
586 and $\frac{P_c}{P_0} - P_c$ show a different behaviour, especially for higher velocity. $\frac{P_c}{P_0}$ presents values higher
587 than $\frac{P_c}{P_0}$ (Figure 11.8). This result is coherent with what has been shown in Figure 5.

588 In other words the interpretation of BTC curves evidences more enhanced nonlinear flow
589 behaviour than the flow tests.

590 For the MIM model in Figure 9 are showed the comparison between the transport time (reciprocal
591 of normalized velocity) and the exchange time (reciprocal of the exchange term) varying the flow
592 rate. As the flow rate increases the difference between transport time and exchange time decreases,
593 and for high values of flow rates they get closer each other (Cherubini et al, 2013a). In analogous
594 way for the ENM4 model in Figure 10 is showed the comparison between the mean travel time for
595 the main path and secondary path varying the injection flow rate. The same behavior as Figure 9 is
596 evident, for high values of flow rates the secondary path reaches the main path in terms of mean
597 travel time. This analogy between MIM and ENM enhances the concept that the mass transfer
598 coefficient is dependent on flow velocity.

599 In Figure 12.1 is reported the relationship between velocity v and injection flow rate Q_0 . Note that,
600 in order to compare the results, the velocities for MIM are evaluated assuming the length of the
601 medium equal to the length of main path ($L = 0.601$ m). Instead for ENM4 model the velocities are
602 evaluated dividing Q_0 for the equivalent area A_{eq} . The models present the same behaviour,
603 and similarly to the mean travel time a change of slope is evident again in correspondence of flow
604 rate equal to $4 \times 10^{-6} \text{ m}^3 \text{ s}^{-1}$. This result confirms the fact that the presence of nonlinear flow regime
605 leads to a delay on solute transport with respect to the values that can be obtained under the
606 assumptions of a linear flow field.

Formatted: English (U.K.), Not Highlight

Formatted: English (U.K.)

Formatted: English (U.K.), Not Highlight

Formatted: English (U.K.)

Formatted: English (U.K.)

Formatted: English (U.K.)

Field Code Changed

Formatted: English (U.K.)

Formatted: Font: Italic

Field Code Changed

Formatted: English (U.K.)

Formatted: English (U.K.)

Field Code Changed

Formatted: English (U.K.)

Formatted: English (U.K.)

Formatted: English (U.K.)

Formatted: English (U.K.)

Field Code Changed

Formatted: English (U.K.)

Field Code Changed

Formatted: English (U.K.)

Field Code Changed

Formatted: English (U.K.)

Formatted: English (U.K.)

Field Code Changed

Formatted: English (U.K.)

Formatted: English (U.K.)

Field Code Changed

Formatted: English (U.K.)

Formatted: Font color: Auto, English (U.K.)

Formatted: English (U.K.)

Formatted: English (U.K.)

Formatted: English (U.K.)

Formatted: Font: Italic, English (U.K.)

Formatted: English (U.K.)

Formatted: Font: Italic, English (U.K.)

Formatted: Font: Italic, English (U.K.)

Formatted: English (U.K.)

Formatted: English (U.K.)

Formatted: English (U.K.)

607 In order to better represent the nonlinear flow regime, Figure 13 shows water pressure as a function
608 of velocity. A change of slope is evident for $v = 1.5 \times 10^{-2} \text{ ms}^{-1}$ which corresponds to the flow rate
609 equal to $4 \times 10^{-6} \text{ m}^3 \text{ s}^{-1}$. $v = 1.5 \times 10^{-3} \text{ m/s}$.

Formatted: English (U.K.)

Formatted: English (U.K.)

Field Code Changed

Formatted: English (U.K.), Highlight

Formatted: English (U.K.)

Formatted: English (U.K.)

610 Moreover as shown in Figure 14 a linear trend of dispersion with the injection flow rates both for
611 MIM and ENM models has been observed. This is coherent with what obtained in the previous
612 study (Cherubini et al. 2013a) where a linear relationship is found between velocity and dispersion
613 both for ADE and MIM models with the conclusion that geometrical dispersion dominated the
614 effects of Aris – Taylor dispersion. The values of the coefficient of dispersion obtained for ENM
615 models do not depend on flow velocity but assume a somehow scattered but fluctuating value.
616 Being α_L values constant, geometrical dispersion dominates the mixing processes along the
617 fracture network. Therefore, the presence of a nonlinear flow regime does not prove to exert any
618 influence on dispersion except for high velocities for the ENM model where a weak transitional
619 regime appears.

Formatted: English (U.K.)

620 This does not happen for MIM dispersion values whose rates of increase are smaller than those of
621 ENM dispersion values.

622 The values of dispersion coefficient are in order of magnitude of decimeter, which is comparable
623 with the values obtained for darcian condition (Qian et al, 2011). and the dispersion values of MIM
624 are much lower than those of ENM.

625 This may be attributable to the fact that the MIM separates solute spreading into dispersion in
626 mobile region and mobile-immobile mass transfer. The dispersive effect is therefore partially taken
627 into account by the mass transfer between the mobile zone and the immobile zone (Qian et al, 2011;
628 Gao et al, 2009).

629 Conclusion

630 Flow and tracer test experiments ~~were have been carried out~~ conducted in a fracture network. The aim
631 of the present study is that of comparing the performances and reliabilities of two model paradigms:
632 the Mobile - Immobile Model (MIM) and the Explicit Network Model (ENM) to describe
633 conservative tracer transport in a fractured rock sample.

Formatted: English (U.K.)

634 Fluid flow experiments show a not negligible nonlinear behaviour of flow best described by the
635 Forchheimer law. The solution of the flow field for each single fracture highlighted that the
636 probabilities of water distribution between the main and the secondary path are not constant but
637 decrease as the injection flow rate increases. In other words varying the injection flow rate the
638 conductance of the main path decreases more rapidly than the conductance of the secondary path.

639 The BTCs curves determined by transport experiments ~~were-have been~~ fitted by MIM model and
640 three versions of ENM model (ENM2, ENM3, ENM4) which differ on the basis of the assumptions
641 made on the parameters P_Q and P_C . All models ~~show~~prove a satisfactory fitting. The ENM4 model
642 provides the best fit which is expectable because it has more fitting parameters than ENM2 and
643 ENM3, thus it is more flexible. Secondly, compared to MIM model, it takes explicitly into account
644 the presence of the secondary path. Furthermore for the ENM model the parameter P_Q decreases
645 more rapidly varying the injection flow rate than the same parameter ~~evaluated-determined~~ by flow
646 tests. The relationship between transport time and exchange time for MIM model and mean travel
647 time for main path and secondary path for the ENM4 model varying the injection flow rate has
648 shown similarity of behaviour: for higher values of flow rate the difference between transport time
649 and exchange time decreases and the secondary path reaches the main path in terms of mean travel
650 time. This analogy between MIM and ENM explains the fact that the mass transfer coefficient is
651 dependent on flow velocity. The mass transfer coefficient increases as the importance of secondary
652 path over the main path increases.

653 The velocity values evaluated for MIM and ENM model show the same relationship with the
654 injection flow rate. In particular a change of slope is evident in correspondence of the flow rate
655 equal to $4 \times 10^{-6} \text{ m}^3\text{s}^{-1}$. This behaviour occurs before the critical flow rate estimated by flow tests
656 equal to $6.3 \times 10^{-6} \text{ m}^3\text{s}^{-1}$. Therefore the interpretation of BTCs curves evidences ~~s~~d more enhanced
657 nonlinear behaviour than flow tests. These results confirm the fact that the presence of transitional
658 flow regime leads to a delay on solute transport with respect to the values that can be obtained
659 under the assumption of a linear flow field (Cherubini et al., 2013a).

660 As concerns dispersion, a linear trend varying the velocity for both MIM and ENM models has been
661 observed -coherently with the previous results- (Cherubini et al., 2013a), the MIM model
662 underestimating the dispersion respect to ENM4 model.

663 The dispersivity values obtained for ENM models do not depend on flow velocity but assume a
664 somehow scattered but fluctuating value. Being α_L values constant, geometrical dispersion
665 dominates the mixing processes along the fracture network. Therefore, the presence of a nonlinear
666 flow regime does not prove to exert any influence on dispersion except for high velocities for the
667 ENM model where a weak transitional regime seems to appear. This result demonstrates that for our
668 experiment geometrical dispersion still dominates Taylor dispersion.

669 A major challenge for tracer tests modeling in fractured media is the adequate choice of the
670 modeling approach for each different study scale.

Formatted: English (U.K.)

Formatted: Font: Italic, English (U.K.)

Formatted: English (U.K.)

Formatted: Font: Italic, English (U.K.)

Formatted: English (U.K.)

Formatted: English (U.K.)

Formatted: Font: Italic, English (U.K.)

Formatted: English (U.K.)

Formatted: English (U.K.)

Formatted: English (U.K.)

671 When dealing with large scales, tracer tests breakthrough curves are generally modeled by a
672 relatively small number of model parameters (Becker and Shapiro, 2000).

673 At laboratory scale, the definition of the network of fractures by means of discrete approaches
674 (DFN) can permit to identify transport pathways and mass transport coefficients, in order to better
675 define heterogeneous advective phenomena (Cherubini et. al, 2013b).

Formatted: English (U.K.)

676 At an intermediate local field scale (1-100m), recognition that heterogeneous environments contain
677 fast and slow paths led to the development of the MIM formulation applied successfully in a variety
678 of hydrogeologic settings. However, the assumed velocity partitioning into flowing and not-flowing
679 zones is not an accurate representation of the true velocity field (Gao et al., 2009). Especially when
680 the rock mass is sparsely fractured, the breakthrough curves are characterized by early breakthrough
681 and long tailing behaviour, and a simple mobile-immobile conceptualization may be an over
682 simplification of the physical transport phenomenon.

Formatted: English (U.K.)

683 Solute transport in fractured aquifers characterized by highly non-Fickian behaviour, is therefore
684 better described by an Explicit Network Model rather than by a simple MIM. Applying a discrete
685 model in such a case can permit to determine if transport occurs through one or several fractures
686 and if multiple arrivals are caused by fracture heterogeneity, in such a way as to yield a more robust
687 interpretation of the subsurface transport regime.

Formatted: English (U.K.)

688 In such a context, geophysical imaging may provide detailed information about subsurface structure
689 and dynamics (Dorn et al, 2012). Differently from “black box” one dimensional models the
690 definition of the network of fracture may allow to better characterize the nonlinear flow behavior
691 and its influence on solute propagation in a fractured medium at bench scale (Cherubini et. al,
692 2013b).

693

694 **References**

695 Bauget, F., Fourar, M.: Non-Fickian dispersion in a single fracture. J. Contam. Hydrol. 100(3-4),
696 137–148 (2008). doi:10.1016/j.jconhyd.2008.06.005

697 Bauget, F. and Fourar, M.: Non-Fickian dispersion in a single fracture, J. Contam. Hydrol., 100,
698 137–148, doi:10.1016/j.jconhyd.2008.06.005, 2008.

699 Bear, J.: Dynamics of Fluids in Porous Media, Elsevier, New York, 1972.

700 [Bear, J. and Berkowitz, B.: Groundwater flow and pollution in fractured rock aquifers, in:](#)
 701 [Developments in Hydraulic Engineering, vol. 4, edited by: Novak, P., Elsevier Applied Science](#)
 702 [Publishers Ltd., New York, 175–238, 1987.](#)

703 [Becker, M. W. and Shapiro, A. M.: Tracer transport in fractured crystalline rock: evidence of](#)
 704 [nondiffusive breakthrough tailing, Water Resour. Res., 36, 1677–1686,](#)
 705 [doi:10.1029/2000WR900080, 2000.](#)

706 [Berkowitz, B.: Characterizing flow and transport in fractured geological media: a review, Adv.](#)
 707 [Water Resour., 25, 861–884, 2002.](#)

708 [Berkowitz, B., Cortis, A., Dentz, M., and Scher, H.: Modeling non-Fickian transport in geological](#)
 709 [formations as a continuous time random walk, Rev. Geophys., 44, RG2003,](#)
 710 [doi:10.1029/2005RG000178, 2006.](#)

711 [Bodin, J., Delay, F., and de Marsily, G.: Solute transport in a single fracture with negligible matrix](#)
 712 [permeability: 1. fundamental mechanisms, Hydrogeol. J., 11, 418–433, 2003.](#)

713 [Bodin, J., Porel, G., Delay, F., Ubertosi, F., Bernard, S., and de Dreuzy, J.: Simulation and analysis](#)
 714 [of solute transport in 2-D fracture/pipe networks: the SOLFRAC program, J. Contam. Hydrol., 89,](#)
 715 [1–28, 2007.](#)

716 [Cherubini, C.: A modeling approach for the study of contamination in a fractured aquifer, in:](#)
 717 [Geotechnical and Geological Engineering, vol. 26, Springer, the Netherlands, 519–533, 2008.](#)

718 [Cherubini, C. and Pastore, N.: Modeling contaminant propagation in a fractured and karstic aquifer,](#)
 719 [Fresen. Environ. Bull., 19, 1788–1794, 2010.](#)

720 [Cherubini, C. and Pastore, N.: Critical stress scenarios for a coastal aquifer in southeastern Italy,](#)
 721 [Nat. Hazards Earth Syst. Sci., 11, 1381–1393, doi:10.5194/nhess-11-1381-2011, 2011.](#)

722 [Cherubini, C., Giasi, C.I., Pastore, N.: Application of Modelling for Optimal Localisation of](#)
 723 [Environmental Monitoring Sensors, Proceedings of the Advances in sensor and Interfaces \(IWASI\),](#)
 724 [Trani, Italy, 2009, 222-227, 2009](#)

725 [Cherubini, C., Giasi, C. I., and Pastore, N.: Bench scale laboratory tests to analyze non-linear flow](#)
 726 [in fractured media, Hydrol. Earth Syst. Sci., 16, 2511–2522, doi:10.5194/hess-16-2511-2012, 2012.](#)

727 [Cherubini, C., Giasi, C. I., and Pastore, N.: Evidence of non-Darcy flow and non-Fickian transport](#)
728 [in fractured media at laboratory scale, Hydrol. Earth Syst. Sci., 17, 2599–2611, doi:10.5194/hess-](#)
729 [17-2599-2013, 2013a.](#)

730 [Cherubini, C., Giasi, C. I., and Pastore, N.: Fluid flow modeling of a coastal fractured karstic](#)
731 [aquifer by means of a lumped parameter approach, Environ. Earth Sci., 70, 2055–2060, 2013b.](#)

732 [Delay, F. and Bodin, J.: Time domain random walk method to simulate transport by advection–](#)
733 [dispersion and matrix diffusion in fracture networks, Geophys. Res. Lett., 28, 4051–4054, 2001.](#)

734 [De Smedt, F. and Wierenga, P. J.: Solute transfer through columns of glass beads, Water Resour.](#)
735 [Res., 20, 225–232, 1984.](#)

736 [Feehley, C. E., Zheng, C., and Molz, F. J.: A dual-domain mass transfer approach for modeling](#)
737 [solute transport in heterogeneous aquifers: Application to the Macrodispersion Experiment](#)
738 [\(MADE\) site, Water Resour. Res., 36, 2501–2515, 2010.](#)

739 [Forchheimer, P.: Wasserbewegung durch Boden, Z. Verein Deut. Ing., 45, 1781–1788, 1901.](#)

740 [Gaudet, J. P., Jégat, H., Vachaud, G., and Wierenga, P. J.: Solute transfer, with exchange between](#)
741 [mobile and stagnant water, through unsaturated sand, Soil Sci. Soc. Am. J., 41, 665–671, 1977.](#)

742 [Geiger, S., Cortis, A., and Birkholzer, J. T.: Upscaling solute transport in naturally fractured porous](#)
743 [media with the continuous time random walk method, Water Resour. Res., 46,](#)
744 [doi:10.1029/2010WR009133, 2010.](#)

745 [Gylling, B., Moreno, L., and Neretnieks, I.: Transport of solute in fractured media, based on a](#)
746 [channel network model, in: Proceedings of Groundwater Quality: Remediation and Protection](#)
747 [Conference, edited by: Kovar, K. and Krasny, J., 14–19 May, Prague, 107–113, 1995.](#)

748 [Jiménez-Hornero, F. J., Giráldez, J. V., Laguna, A., and Pachepsky, Y.: Continuous time](#)
749 [randomwalks for analyzing the transport of a passive tracer in a single fissure, Water Resour. Res.,](#)
750 [41, W04009, doi:10.1029/2004WR003852, 2005.](#)

751 [Kamra, S. K., Lennartz, B., van Genuchten, M. T., and Widmoser, P.: Evaluating non-equilibrium](#)
752 [solute transport in small soil columns, J. Contam. Hydrol., 48, 189–212, 2001.](#)

753 [Klov, T.: High-velocity flow in fractures, Dissertation for the partial fulfillment of the requirements](#)
754 [for the degree of doktor ingénieur Norwegian University of Science Technology Department of](#)
755 [Petroleum Engineering and Applied Geophysics, Trondheim, 2000.](#)

Formatted: German (Germany)

756 Liu, H. H., Mukhopadhyay, S., Spycher, N., and Kennedy, B. M.: Analytical solutions of tracer
757 transport in fractured rock associated with precipitation-dissolution reactions, Hydrogeol. J.,19,
758 1151–1160, 2011.

759 Moutsopoulos, K. N., Papaspyros, I. N. E., and Tsihrintzis, V. A.: Experimental investigation of
760 inertial flow processes in porous media, J. Hydrol., 374, 242–254, 2009.

761 Mulla, D. J. and Strock, J. S.: Nitrogen transport processes in soil, in: Nitrogen in agricultural
762 systems, edited by: Schepers, J. S. and Raun, W. R., Agron. Monogr. 49, ASA, CSSA, SSSA,
763 Madison, WI, 401–436, 2008.

764 Neretnieks, I., Eriksen, T., and Tahtinen, P.: Tracer movement in a single fissure in granitic rock:
765 some experimental results and their interpretation, Water Resour. Res., 18, 849–858,
766 doi:10.1029/WR018i004p00849, 1982.

767 ~~Bear, J., 1972. Dynamics of Fluids in Porous Media, Elsevier, New York.~~

768 ~~Bear, J. and B. Berkowitz (1987). Groundwater flow and pollution in fractured rock aquifers, in~~
769 ~~Developments in Hydraulic Engineering, Volume 4, pp. 175–238, P. Novak (ed.), Elsevier Applied~~
770 ~~Science Publishers Ltd., New York.~~

771 ~~Becker, M.W., Shapiro, A.M.: Tracer transport in fractured crystalline rock: evidence of~~
772 ~~nondiffusive breakthrough tailing. Water Resour. Res. 36(7), 1677–1686 (2000).~~
773 ~~doi:10.1029/2000WR900080~~

774 ~~Berkowitz B. (2002) Characterizing flow and transport in fractured geological media: A review.~~
775 ~~Advances in Water Resources Volume 25, Issues 8–12, August–December 2002, Pages 861–884~~

776 ~~Berkowitz, B., Cortis, A., Dentz, M., Scher, H.: Modeling non Fickian transport in geological~~
777 ~~formations as a continuous time random walk. Rev. Geophys. 44, RG2003 (2006).~~
778 ~~doi:10.1029/2005RG000178~~

779 ~~Bodin J., Delay F., de Marsily G. (2003) Solute transport in a single fracture with negligible matrix~~
780 ~~permeability: 1. fundamental mechanisms. Hydrogeology Journal August 2003, Volume 11, Issue~~
781 ~~4, pp 418–433~~

782 ~~Bodin J, Porel G, Delay F, Ubertosi F, Bernard S, de Dreuzy J (2007) Simulation and analysis of~~
783 ~~solute transport in 2D fracture/pipe networks: The SOLFRAC program Journal of Contaminant~~
784 ~~Hydrology 89 (2007) 1–28~~

Formatted: English (U.S.)

Formatted: English (U.K.)

785 ~~Cherubini Claudia (2008): A Modeling Approach For The Study of Contamination in a Fractured~~
786 ~~Aquifer. In:Geotechnical And Geological Engineering. Vol. 26 N.5, Pp. 519-533 ISSN: 0960-3182.~~
787 ~~Springer Netherlands.~~

788 ~~Cherubini, C., Pastore, N. (2010). Modeling contaminant propagation in a fractured and karstic~~
789 ~~aquifer. Fresenius Environmental Bulletin. 19(9) pp. 1788-1794.~~

Formatted: Italian (Italy)

Formatted: English (U.K.)

790 ~~Claudia Cherubini, Nicola Pastore (2011) Critical stress scenarios for a coastal aquifer in~~
791 ~~southeastern Italy. Natural Hazards and Earth System Sciences NHESS 11, 1381-1393, 2011~~
792 ~~doi:10.5194/nheiss-11-1381-2011 ISSN: 1561-8633 eISSN: 1684-9981 © Author(s) 2011. CC~~
793 ~~Attribution 3.0 License.~~

Formatted: Italian (Italy)

Formatted: English (U.S.)

794 ~~Cherubini, C., Giasi, C. I., Pastore, N. (2012). Bench-scale laboratory tests to analyze non-linear~~
795 ~~flow in fractured media. Hydrology and Earth System Sciences. 16(8), pp. 2511-2622.~~

Formatted: English (U.K.)

796 ~~Cherubini, C., Giasi, C. I., Pastore, N. (2013a). Evidence of non-Darcy flow and non-Fickian~~
797 ~~transport in fractured media at laboratory scale. Hydrology and Earth System Sciences. 17(7), pp.~~
798 ~~2599-2611.~~

Formatted: English (U.K.)

799 ~~Cherubini, C., Giasi, C. I., Pastore, N. (2013b). Fluid flow modeling of a coastal fractured karstic~~
800 ~~aquifer by means of a lumped parameter approach. Environmental Earth Sciences, November 2013,~~
801 ~~Volume 70, Issue 5, pp-2055-2060~~

Formatted: English (U.K.)

802 ~~De Smedt, F., and P. J. Wierenga, Solute transfer through columns of glass beads, Water Resour.~~
803 ~~Res., 20, 225-232, 1984.~~

804 ~~Delay, F., Bodin, J., (2001). Time domain random walk method to simulate transport by advection-~~
805 ~~dispersion and matrix diffusion in fracture networks. Geophys. Res. Lett. 28 (21), 4051-4054.~~

806 ~~Feehley C.E, Zheng C. and Molz F.J. (2010) A dual domain mass transfer approach for modeling~~
807 ~~solute transport in heterogeneous aquifers: Application to the Macrodispersion Experiment~~
808 ~~(MADE) site Water Resources Research Volume 36, Issue 9, pages 2501-2515, September 2000~~

809 ~~Forchheimer, P. (1901). Wasserbewegung durch Boden. Zeitschrift Verein Deutscher Ingenieure~~
810 ~~vol 45, 1781-1788~~

811 ~~Gaudet, J.P., H. Jégat, G. Vachaud and P.J. Wierenga, 1977. Solute transfer, with exchange between~~
812 ~~mobile and stagnant water, through unsaturated sand. Soil Sci. Soc. Amer. J. 41: pp. 665-671~~

Formatted: English (U.K.)

813 Geiger S., Cortis A., and J. T. Birkholzer (2010) Upscaling solute transport in naturally fractured
814 porous media with the continuous time random walk method Water Resources Research Volume
815 46, Issue 12, December 2010 DOI: 10.1029/2010WR009133

816 Gylling B.; Moreno L.; and Neretnieks I. (1995) Transport of solute in fractured media, based on a
817 channel network model. In Proceedings of Groundwater Quality: Remediation and Protection
818 Conference, Eds K. Kovar and J. Krasny, 107–113, Prague May 14–19, 1995.

819 Jiménez-Hornero, F.J., Giráldez, J.V., Laguna, A., Pachepsky, Y.: Continuous time random walks for
820 analyzing the transport of a passive tracer in a single fissure. Water Resour. Res. 41, W04009
821 (2005). doi:10.1029/2004WR003852

822 Izbash, S. (1931). *O filtracii v Kropnozernstom Materiale*. Leningrad USSR, [in Russian].

823 Kamra, S. K., Lennartz, B., van Genuchten, M. T., and Widmoser, P.: Evaluating non-equilibrium
824 solute transport in small soil columns, J. Contam. Hydrol., 48, 189–212, 2001.

825 Klov, T. (2000). *High velocity flow in fractures*. Dissertation for the partial fulfillment of the
826 requirements for the degree of doktor ingeniør Norwegian University of Science Technology
827 Department of Petroleum Engineering and Applied Geophysics Trondheim.

828 Liu H. H., Mukhopadhyay S., Spycher N., Kennedy B. M. (2011) Analytical solutions of tracer
829 transport in fractured rock associated with precipitation-dissolution reactions Hydrogeology Journal
830 September 2011, Volume 19, Issue 6, pp 1151–1160

831 Moutopoulos K.N., Papaspyros I.N.E., Tsihrintzis V.A. Experimental investigation of inertial flow
832 processes in porous media J. Hydrol., 374 (3–4) (2009), pp. 242–254

833 Mulla, D.J. and J.S. Strock. 2008. Nitrogen transport processes in soil. p. 401–436. In J.S. Schepers
834 and W.R. Raun (ed.) Nitrogen in agricultural systems. Agron. Monogr. 49. ASA, CSSA,
835 SSSA, Madison, WI.

836 Neretnieks, I., Eriksen, T., Tahtinen, P.: Tracer movement in a single fissure in granitic rock: some
837 experimental results and their interpretation. Water Resour. Res. 18(4), 849–858 (1982).
838 doi:10.1029/WR018i004p00849

839 Neuman, S. P. (2005) Trends, prospects and challenges in quantifying flow and transport through
840 fractured rocks Hydrogeology Journal March 2005, Volume 13, Issue 1, pp 124–147

841 ~~Nkedi-Kizza, P., J. W. Biggar, M. T. van Genuchten, P. J. Wierenga, H. M. Selim, J. M. Davidson~~
842 ~~and D. R. Nielsen. 1983. Modeling tritium and chloride 36 transport through an aggregated oxisol.~~
843 ~~Water Resour. Res. 19:691-700~~

844 ~~Nowamooz A., Radilla R., Fourar M., Berkowitz B. (2013) Non-Fickian Transport in Transparent~~
845 ~~Replicas of Rough-Walled Rock Fractures Transport in Porous Media July 2013, Volume 98, Issue~~
846 ~~3, pp 651-682 DOI 10.1007/s11242-013-0165-7~~

847 ~~Qian, J. Z., Chen, Z., Zhan, H. B., and Luo, S. H.: Solute transport in a filled single fracture under~~
848 ~~non-Darcian flow, Int. J. Rock Mech. Min., 48, 132-140, 2011.~~

849 ~~Schumer R., Benson D. A., Baeumer B. (2003) Fractal mobile/immobile solute transport. Water~~
850 ~~Resources Research Volume 39, Issue 10, October 2003 DOI: 10.1029/2003WR002141~~

851 ~~Selim, H. M., and L. Ma, Transport of reactive solutes in soils: A modified two-region approach,~~
852 ~~Soil Sci. Soc. Am. J. 59, 75-82, 1995~~~~Valocchi, A.J. (1985) Validity of the local equilibrium~~
853 ~~assumption for modeling sorbing solute transport through homogeneous soils. Wat. Resour. Res.~~
854 ~~21(6), 808-820~~

855 ~~Van Genuchten M. Th. And J. Wierenga (1976): Mass transfer studies in sorbing porous media, I-~~
856 ~~Analytical solutions, SSSA Proceedings 40 (4), 473-480.~~~~Zafarani A., Detwiler R. L. (2013) An~~
857 ~~efficient time-domain approach for simulating Pe-dependent transport through fracture intersections~~
858 ~~Advances in Water Resources 53 (2013) 198-207~~

859 ~~Zhang, Z., Nemeik J. (2013) Fluid flow regimes and nonlinear flow characteristics in deformable~~
860 ~~rock fractures Journal of Hydrology, Volume 477, 16 January 2013, Pages 139-151~~

Formatted: English (U.K.)

Formatted: English (U.K.)

Formatted: English (U.K.)

Formatted: English (U.K.)

Formatted: English (U.K.)

Formatted: English (U.K.)

Formatted: English (U.K.)

MIM 1

n°	Q (m ³ /s)×10 ⁻⁶	v/L (s ⁻¹)×10 ⁻²	D/L ² (s ⁻¹)×10 ⁻²	α (s ⁻¹)×10 ⁻²	β (-)	RMSE	r ²
1	1.319	0.73 ± 0.05	0.15 ± 0.01	0.43 ± 0.09	0.95 ± 0.14	0.022	0.979
5	2.209	1.05 ± 0.05	0.16 ± 0.01	0.50 ± 0.12	0.51 ± 0.07	0.021	0.991
10	2.731	1.26 ± 0.05	0.18 ± 0.01	0.60 ± 0.12	0.51 ± 0.06	0.021	0.994
15	3.084	1.74 ± 0.06	0.19 ± 0.01	1.03 ± 0.16	0.56 ± 0.05	0.023	0.995
20	3.365	1.75 ± 0.06	0.20 ± 0.01	1.06 ± 0.17	0.54 ± 0.05	0.022	0.996
25	3.681	2.49 ± 0.10	0.25 ± 0.02	1.67 ± 0.32	0.51 ± 0.06	0.030	0.995
30	4.074	2.57 ± 0.11	0.26 ± 0.02	1.67 ± 0.35	0.50 ± 0.06	0.033	0.994
35	4.536	2.25 ± 0.09	0.21 ± 0.02	1.58 ± 0.29	0.57 ± 0.06	0.031	0.994
40	5.382	3.20 ± 0.13	0.26 ± 0.02	2.68 ± 0.44	0.61 ± 0.06	0.035	0.994
45	5.895	3.32 ± 0.15	0.26 ± 0.02	2.82 ± 0.50	0.57 ± 0.06	0.036	0.995
50	6.168	3.02 ± 0.15	0.26 ± 0.02	2.52 ± 0.52	0.51 ± 0.07	0.031	0.996
55	8.345	3.54 ± 0.29	0.35 ± 0.04	3.05 ± 1.07	0.41 ± 0.11	0.038	0.995

Formatted Table

Formatted: English (U.K.)

MIM 1

n°	Q (m ³ /s)×10 ⁻⁶	v/L (s ⁻¹)×10 ⁻²	D/L ² (s ⁻¹)×10 ⁻²	α (s ⁻¹)	β (-)	RMSE	r ²
1	1.3194	0.73 ± 0.0453	0.15 ± 0.0103	0.004 ± 0.0009	0.95 ± 0.1442	0.0220	0.9786
5	2.2090	1.05 ± 0.0482	0.16 ± 0.0096	0.005 ± 0.0012	0.51 ± 0.0705	0.0213	0.9915
10	2.7312	1.26 ± 0.0478	0.18 ± 0.0095	0.006 ± 0.0012	0.51 ± 0.0596	0.0212	0.9938
15	3.0842	1.74 ± 0.0580	0.19 ± 0.0105	0.010 ± 0.0016	0.56 ± 0.0526	0.0223	0.9950
20	3.3648	1.75 ± 0.0594	0.20 ± 0.0104	0.011 ± 0.0017	0.54 ± 0.0511	0.0220	0.9956
25	3.6813	2.49 ± 0.1037	0.25 ± 0.0166	0.017 ± 0.0032	0.51 ± 0.0587	0.0304	0.9948
30	4.0735	2.57 ± 0.1127	0.26 ± 0.0182	0.017 ± 0.0035	0.50 ± 0.0617	0.0323	0.9940
35	4.5356	2.25 ± 0.0942	0.21 ± 0.0153	0.016 ± 0.0029	0.57 ± 0.0626	0.0310	0.9936
40	5.3824	3.20 ± 0.1324	0.26 ± 0.0199	0.027 ± 0.0044	0.61 ± 0.0627	0.0349	0.9944
45	5.8945	3.32 ± 0.1455	0.26 ± 0.0208	0.028 ± 0.0050	0.57 ± 0.0634	0.0358	0.9946
50	6.1684	3.02 ± 0.1478	0.26 ± 0.0205	0.025 ± 0.0052	0.51 ± 0.0673	0.0312	0.9955
55	8.3455	3.54 ± 0.2916	0.35 ± 0.0363	0.030 ± 0.0107	0.41 ± 0.1060	0.0376	0.9948

Formatted: English (U.K.)

Formatted: English (U.K.)

Formatted: English (U.K.)

Formatted: English (U.K.)

Formatted: English (U.K.)

Formatted: English (U.K.)

Formatted: English (U.K.)

Formatted: English (U.K.)

Formatted: English (U.K.)

Formatted: English (U.K.)

Formatted: English (U.K.)

Formatted: English (U.K.)

Formatted: English (U.K.)

Formatted: English (U.K.)

Formatted: English (U.K.)

Table 11. Estimated values of parameters, root mean square error RMSE and determination coefficient r² for mobile – immobile model MIM at different injection flow rates in the fractured medium.

Formatted: Caption

ENM 2

n°	Q (m ³ /s)×10 ⁻⁶	ω _{eq} (m ²)×10 ⁻⁴	α _l (m)×10 ⁻¹	RMSE	R ²
1	1.3194	3.10 ± 0.14	1.92 ± 0.86	0.033	0.952
5	2.2090	3.22 ± 0.04	0.98 ± 0.06	0.020	0.993
10	2.7312	3.29 ± 0.04	0.92 ± 0.05	0.019	0.995
15	3.0842	2.81 ± 0.03	0.79 ± 0.03	0.020	0.996
20	3.3648	3.06 ± 0.03	0.79 ± 0.03	0.019	0.997
25	3.6813	2.35 ± 0.02	0.74 ± 0.03	0.026	0.996
30	4.0735	2.49 ± 0.02	0.75 ± 0.03	0.027	0.996
35	4.5356	3.27 ± 0.04	0.74 ± 0.04	0.028	0.995
40	5.3824	2.76 ± 0.02	0.75 ± 0.02	0.023	0.998

Formatted: Font: Italic

Formatted Table

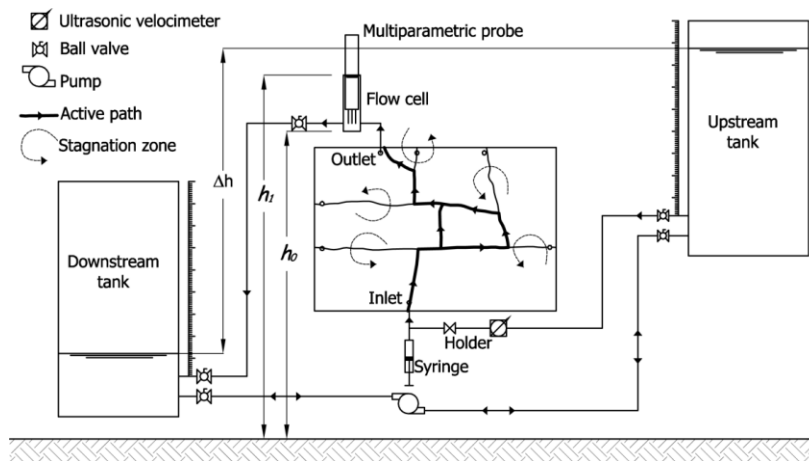
888
889
890
891
892
893

1	1.3194	0.027 ± 0.0013	0.118 ± 0.0107	0.847 ± 0.0195	0.667 ± 0.020	0.0205	0.9815
5	2.2090	0.032 ± 0.0012	0.096 ± 0.0071	0.756 ± 0.0203	0.749 ± 0.026	0.0198	0.9926
10	2.7312	0.033 ± 0.0010	0.092 ± 0.0057	0.750 ± 0.0175	0.756 ± 0.022	0.0190	0.9950
15	3.0842	0.027 ± 0.0006	0.080 ± 0.0040	0.732 ± 0.0129	0.739 ± 0.017	0.0192	0.9966
20	3.3648	0.030 ± 0.0006	0.081 ± 0.0037	0.722 ± 0.0116	0.734 ± 0.016	0.0172	0.9973
25	3.6813	0.023 ± 0.0005	0.080 ± 0.0039	0.703 ± 0.0122	0.739 ± 0.017	0.0200	0.9977
30	4.0735	0.024 ± 0.0006	0.080 ± 0.0042	0.706 ± 0.0135	0.743 ± 0.019	0.0220	0.9974
35	4.5356	0.032 ± 0.0008	0.076 ± 0.0046	0.709 ± 0.0147	0.730 ± 0.020	0.0252	0.9958
40	5.3824	0.026 ± 0.0004	0.076 ± 0.0027	0.699 ± 0.0072	0.703 ± 0.012	0.0163	0.9988
45	5.8945	0.028 ± 0.0003	0.073 ± 0.0022	0.680 ± 0.0061	0.708 ± 0.010	0.0137	0.9992
50	6.1684	0.031 ± 0.0004	0.076 ± 0.0022	0.662 ± 0.0056	0.707 ± 0.011	0.0115	0.9994
55	8.3455	- 0.035 ± 0.0002	- 0.096 ± 0.0013	- 0.628 ± 0.0021	- 0.728 ± 0.006	- 0.0033	- 1.0000

Formatted: English (U.K.)
Formatted: English (U.K.)
Formatted: English (U.K.)
Formatted: English (U.K.)
Formatted: English (U.K.)
Formatted: English (U.K.)
Formatted: English (U.K.)
Formatted: English (U.K.)
Formatted: English (U.K.)
Formatted: English (U.K.)
Formatted: English (U.K.)
Formatted: English (U.K.)
Formatted: English (U.K.)

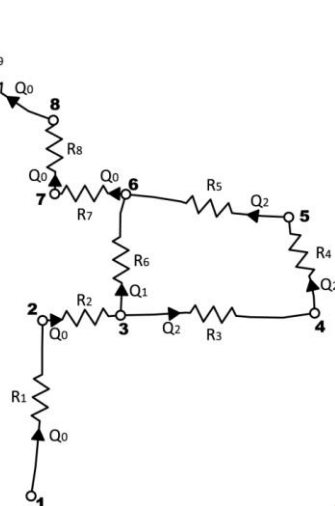
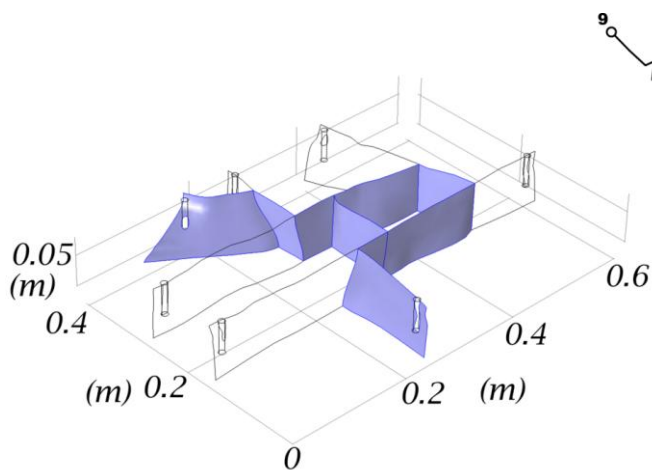
Table 44. Estimated values of parameters, root mean square error RMSE and determination coefficient r^2 for ENM1 at different injection flow rates in the fractured medium.

Formatted: English (U.K.)



Formatted: English (U.K.)

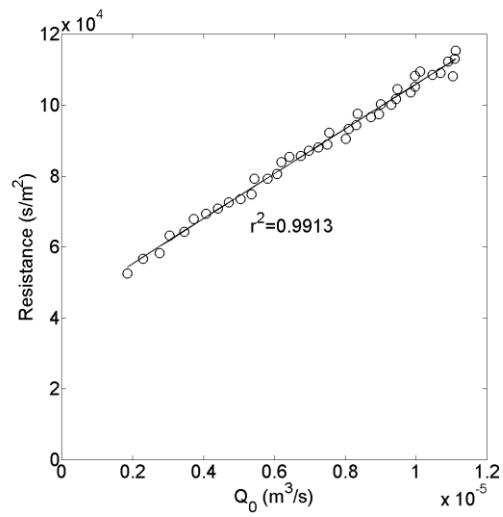
Figure 111. Schematic diagram of experimental setup.



Formatted: English (U.K.)

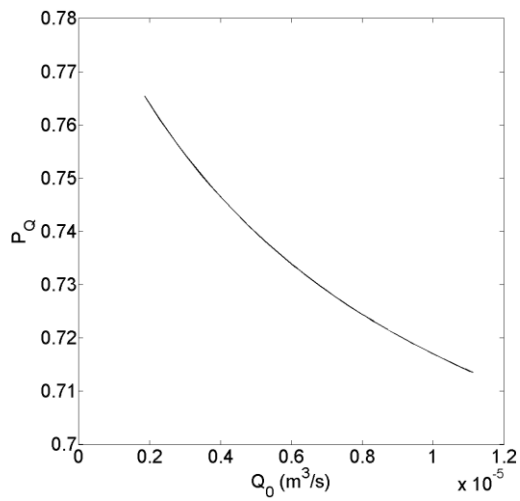
Figure 222. 2d pipe network conceptualization of the fractured medium.

Formatted: English (U.K.)



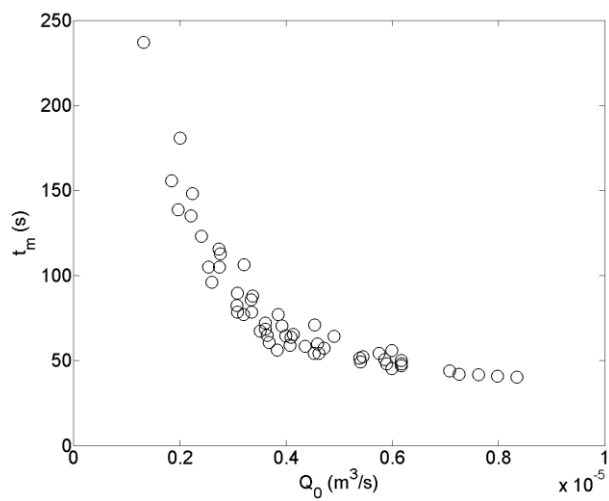
Formatted: English (U.K.)

Figure 333. Average resistance to flow versus injection flow rate Q_0 (m^3/s). The circles represent the experimental values, the straight line represents the resistance to flow evaluated by equation (31).



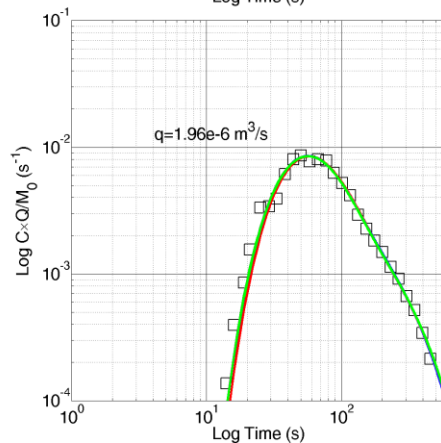
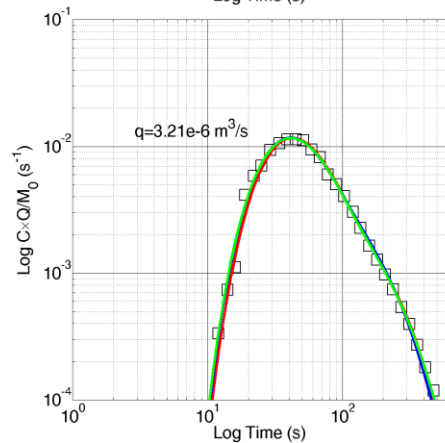
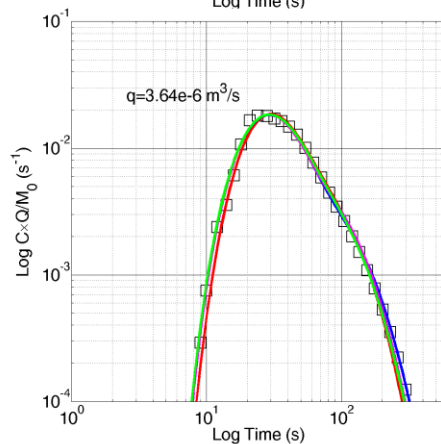
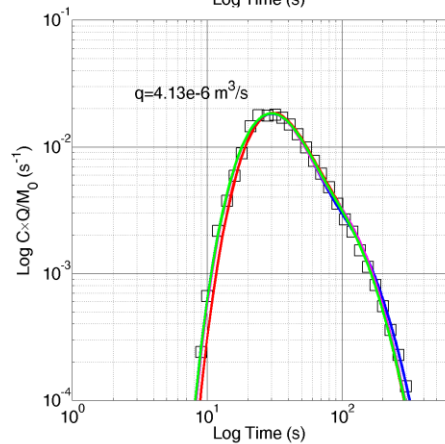
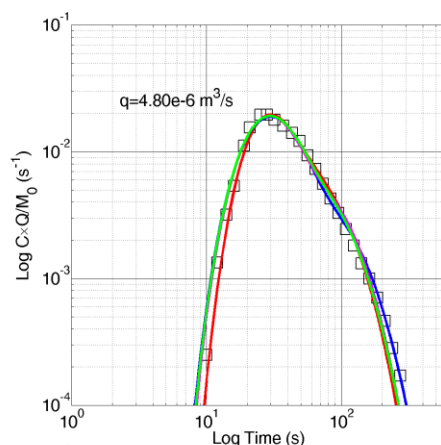
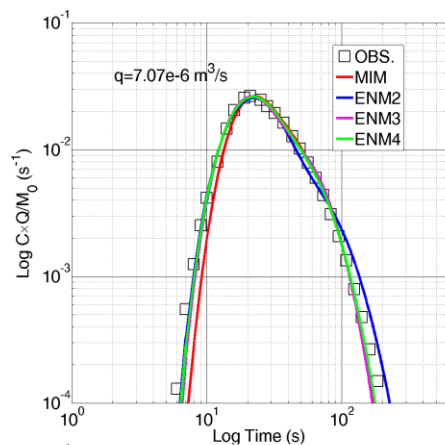
Formatted: English (U.K.)

Figure 444. Probability of water distribution evaluated for main path P_Q versus injection flow rate Q_0 (m^3/s).



Formatted: English (U.K.)

Figure 555. Mean travel time t_m (s) versus injection flow rate Q_0 (m^3/s).



Formatted: Centered

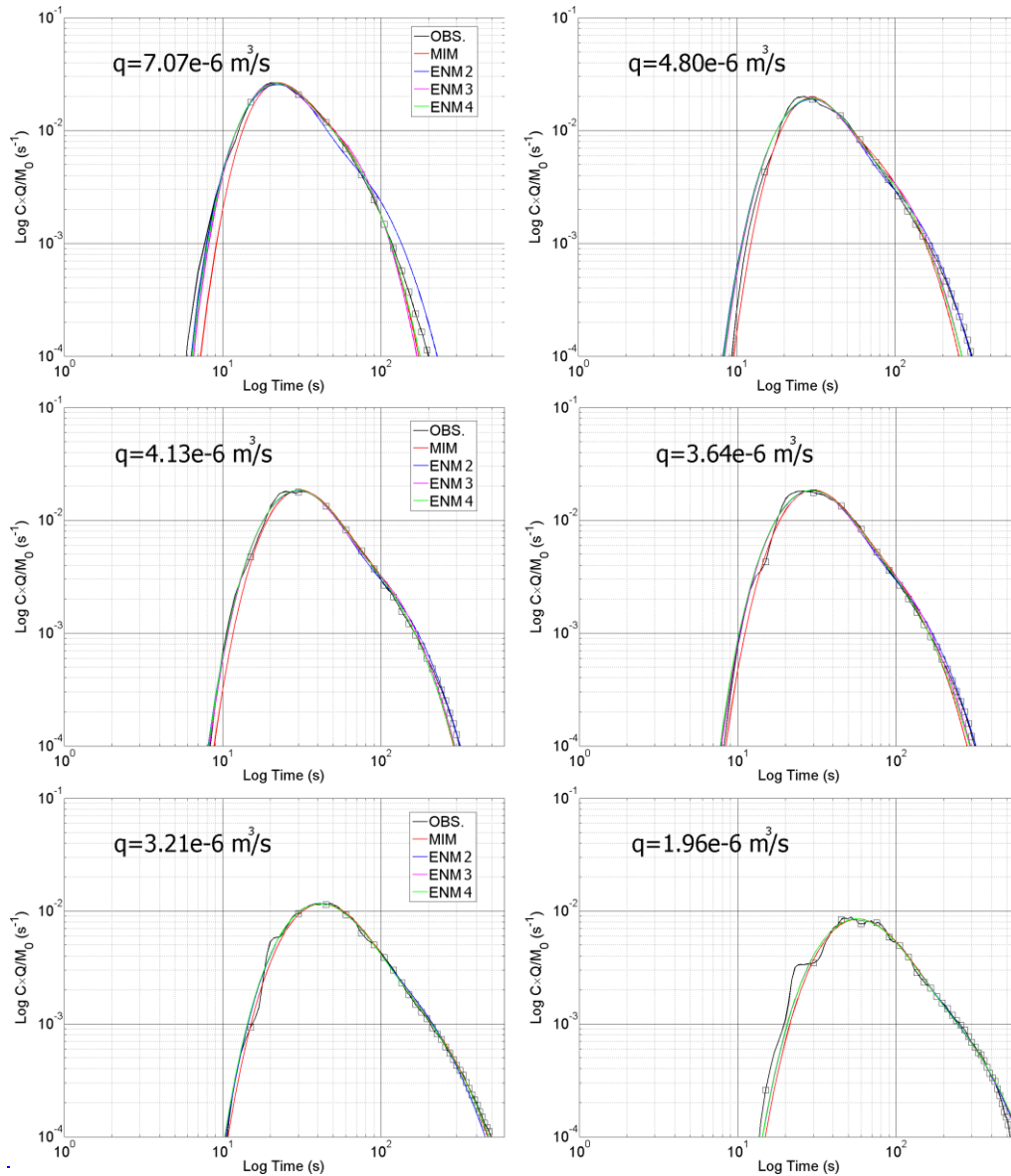
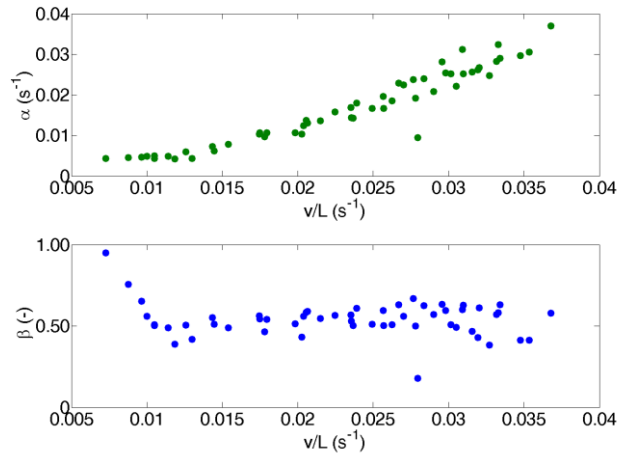


Figure 666. Fitting of breakthrough curves at different injection flow rates using each of the four models (MIM, ENM1, ENM2, ENM3).



Formatted: English (U.K.)

Figure 7. Immobile – mobile ratio (β) as function of normalized velocity v/L (s^{-1}) for MIM model. An outlier is evidenced for $v/L=0.028 s^{-1}$.

Formatted: English (U.K.)

Formatted: English (U.K.)

Formatted: English (U.K.), Superscript

Formatted: English (U.K.)

Formatted: English (U.K.)

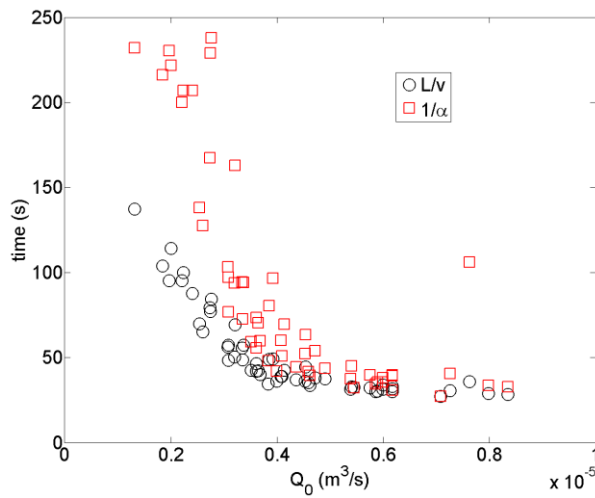


Figure 8. Transport time (L/v) (reciprocal of normalized velocity) and exchange time ($1/\alpha$) (reciprocal of the exchange term) as function of injection flow rate Q_0 (m^3/s) for mobile - immobile model MIM.

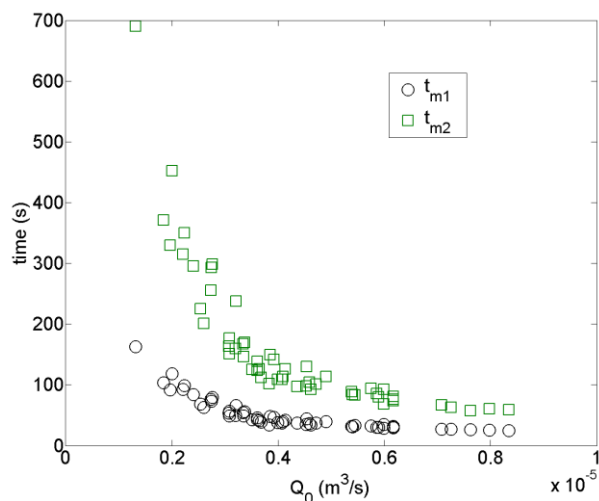
Formatted: English (U.K.)

Formatted: English (U.K.)

Formatted: English (U.K.)

Formatted: English (U.K.)

Formatted: English (U.K.)



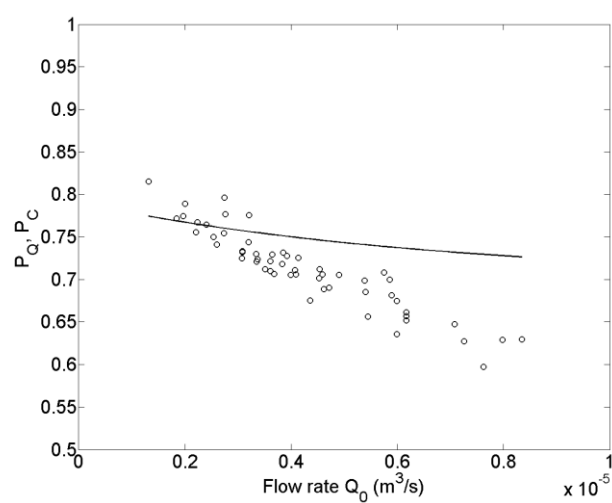
Formatted: English (U.K.)

Figure 9. Travel time for main path t_{m1} (s) and travel time for secondary path t_{m2} (s) for ENM4 as function of injection flow rate Q_0 (m^3/s).

Formatted: English (U.K.)

Formatted: English (U.K.)

Formatted: Normal

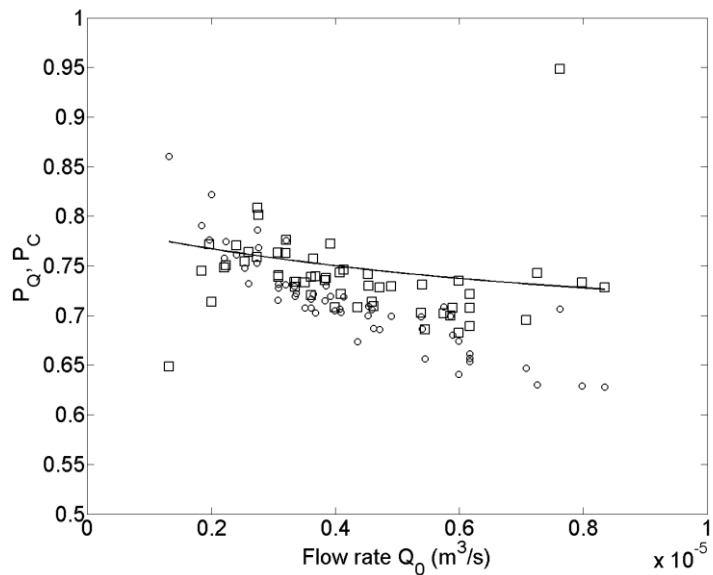


Formatted: English (U.K.)

Figure 10. Comparison between the Probability of water distribution P_O evaluated as the square brackets term in Equation (29) by the flow model (straight line) and P_Q supposed equal to the probability of particle transition $P_C(P_Q)$ for ENM3 (circle) varying the injection flow rate Q_0 (m^3/s).

Formatted: English (U.K.)

Formatted: English (U.K.)



Formatted: English (U.K.)

Figure 8.11. Comparison between the Probability of water distribution P_Q evaluated by the flow model (straight line) and the probability of particle transition P_C (square) and P_Q (circle) for ENM4 varying the injection flow rate Q_0 (m^3/s).

Formatted: English (U.K.)

Formatted: English (U.K.)

Formatted: Normal, Centered

Formatted: English (U.K.)

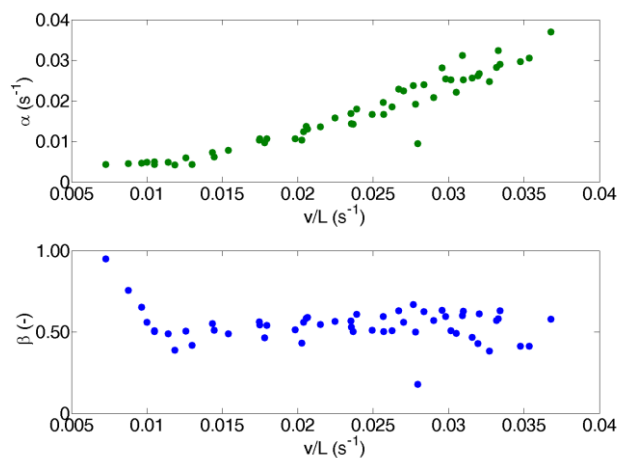


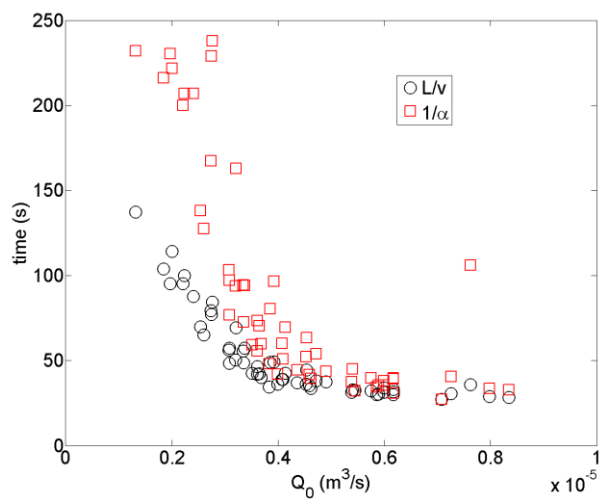
Figure 8.12. Immobile—mobile ratio (β) as function of normalized velocity v/L (s^{-1}) for MIM model.

Formatted: English (U.K.)

Formatted: English (U.K.)

Formatted: English (U.K.)

Formatted: English (U.K.)



Formatted: English (U.K.)

Figure 109. Transport time (L/v) (reciprocal of normalized velocity) and exchange time ($1/\alpha$) (reciprocal of the exchange term) as function of injection flow rate Q_0 (m^3/s) for immobile–mobile model IMM.

Formatted: English (U.K.)

Formatted: English (U.K.)

Formatted: English (U.K.)

Formatted: English (U.K.)

Formatted: English (U.K.)

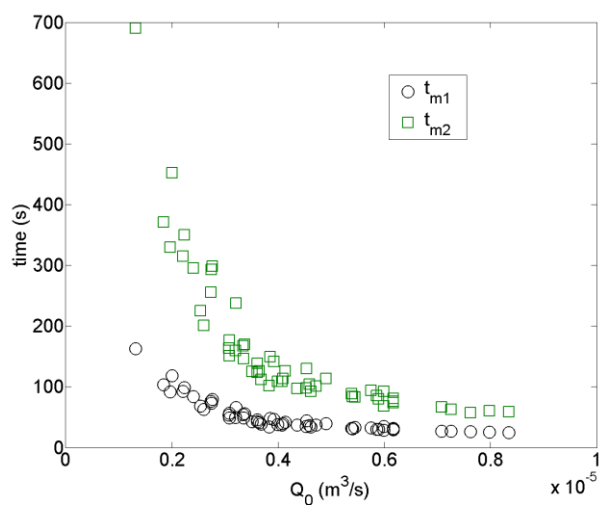
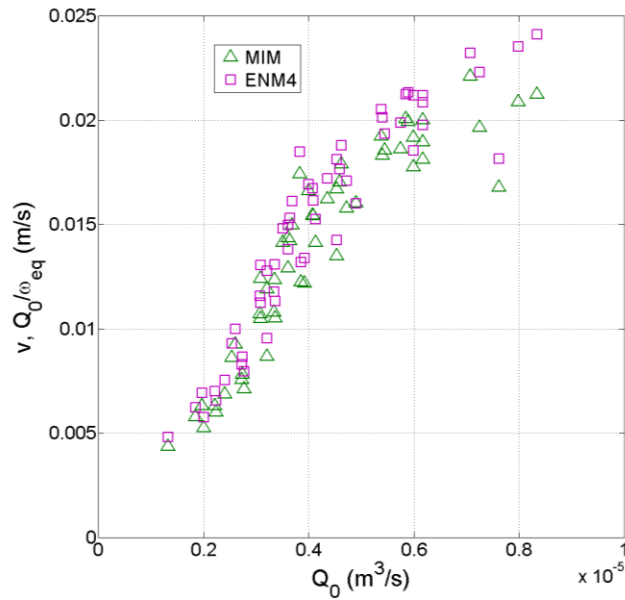


Figure 110. Travel time for main path t_{m1} (s) and travel time for secondary path t_{m2} (s) for ENM2 as function of injection flow rate Q_0 (m^3/s).

Formatted: English (U.K.)

Formatted: English (U.K.)



Formatted: English (U.K.)

Figure 12, velocity v (m/s) as function of the injection flow rate Q_0 (m³/s) for MIM and ENM4 models. Note that for MIM model the v is determined assuming the length of medium equal to the length of main path ($L = 0.601$ m). Instead for the ENM4 model the velocity is determined dividing Q_0 for the equivalent area ω_{eq} .

Formatted: English (U.K.)

Formatted: English (U.K.)

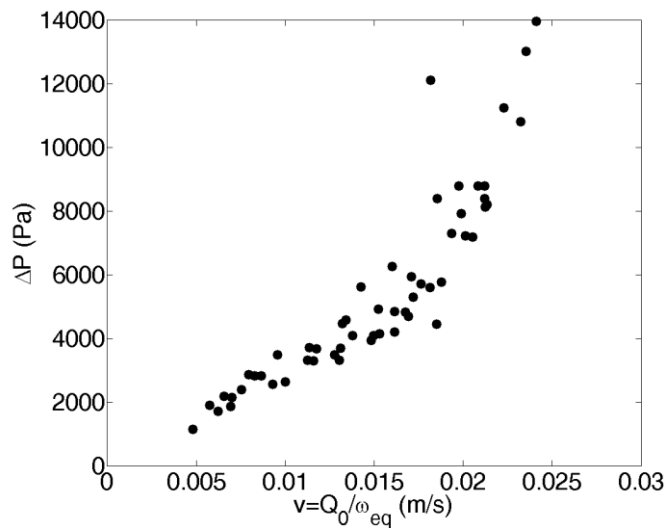
Formatted: English (U.K.)

Formatted: English (U.K.)

Formatted: Normal

Formatted: English (U.K.)

Formatted: Normal, Centered



Formatted: English (U.K.)

Formatted: English (U.K.)

Formatted: English (U.K.)

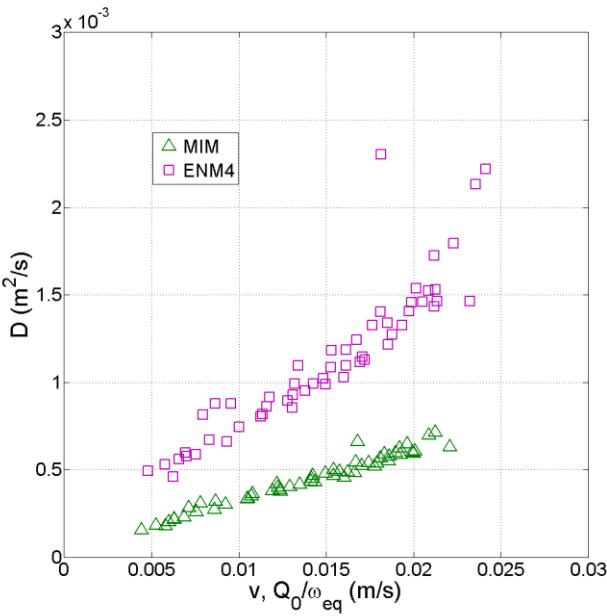
Formatted: English (U.K.)

Formatted: English (U.K.)

Formatted: English (U.K.)

Figure 13, difference of pressure ΔP (Pa) as function of velocity v (m/s) for ENM4. The velocity is determined dividing Q_0 for the equivalent area ω_{eq} .

944



945

946

947

948

Figure 14.14. Dispersion D (m^2/s) as function of velocity for MIM and ENM4 models. Note that for MIM model D is determined assuming the length of the medium equal to the length of the main path ($l=0.601 \text{ m}$). Instead for ENM4 model D is determined as $D=Q_0 \alpha_l / \rho_{eq}$.

Formatted: Normal

Formatted: English (U.K.)

Formatted: Font: Bold, English (U.K.)

Formatted: Font: Bold

Formatted: English (U.K.)

Formatted: English (U.K.)

Formatted: English (U.K.)

Formatted: English (U.K.)

Formatted: English (U.K.)